ESCRT-III acts in scissioning new peroxisomes from the ER

Authors: Fred D. Mast[1,2], Thurston Herricks[1,2], Kathleen M. Strehler[1,2], Leslie R. Miller[1,2], Ramsey A. Saleem[1,2,†], Richard A. Rachubinski[3], and John D. Aitchison[1,2,3,*].

1. Center for Infectious Disease Research, 307 Westlake Avenue North, Suite 500, Seattle, Washington, 98109-5219, United States of America
2. Institute for Systems Biology, 401 Terry Avenue North, Seattle, Washington, 98109-5219, United States of America
3. Department of Cell Biology, University of Alberta, 5-14 Medical Sciences Building, Edmonton, Alberta, T6G 2H7, Canada

† Current address: Amgen, 360 Binney Street, Cambridge, Massachusetts, 02142-1011

Corresponding author:
John D. Aitchison, PhD
Center for Infectious Disease Research
307 Westlake Avenue North, Suite 500
Seattle, Washington, 98109-5219
Tel: (206) 256-7470
Fax: (206) 256-7229
john.aitchison@cidresearch.org

Character count without spaces: 36,651

Keywords: peroxisome biogenesis; ESCRT-III; peroxisomes; preperoxisomal vesicles; ER; peroxin; Snf7; Vps20; Did4; Vps24; Pex3; Pex19

Abbreviations: DOX, doxycycline; DRP, dynamin-related protein; ESCRT, endosomal sorting complexes required for transport; PBD, peroxisome biogenesis disorder; *PEX*, gene encoding a peroxin; PMP, peroxisomal membrane protein; PPV, preperoxisomal vesicle.

Abstract

Dynamic control of peroxisome proliferation is integral to the peroxisome's many functions. A breakdown in the ability of cells to form peroxisomes is linked to many human health issues, including defense against infectious agents, cancer, aging, heart disease, obesity and diabetes, and forms the basis of a spectrum of peroxisomal genetic disorders that cause severe neuropathologies. The ER serves as a source for preperoxisomal vesicles (PPVs) that mature into peroxisomes during de novo peroxisome biogenesis and to support growth and division of existing peroxisomes. However, the mechanism of PPV formation and release from the ER remains poorly understood. Here we show that the evolutionarily ancient endosomal sorting complexes required for transport (ESCRT)-III are peroxisome biogenesis factors that function to cleave PPVs budding from the ER into the cytosol. Using comprehensive morphological and genetic assays of peroxisome formation and function we find that absence of ESCRT-III proteins impedes de novo peroxisome formation and results in an aberrant peroxisome population in vivo. Using a cell-free PPV budding assay we show that ESCRT-III proteins Vps20 and Snf7 are required to release PPVs from the ER. ESCRT-III is therefore a positive effector of membrane scission for vesicles budding both away from and towards the cytosol, a finding that has important implications for the evolutionary timing of emergence of peroxisomes and the rest of the internal membrane architecture of the eukaryotic cell.

53 **Introduction**

54 Peroxisomes are membrane-bound, spherical organelles that are found across eukaryotes
55 (Smith and Aitchison, 2013). All peroxisomes share common mechanisms guiding their
56 biogenesis, division and protein import. The conserved protein products of *PEX* genes, termed
57 peroxins, mediate the formation and maintenance of peroxisomes (Distel et al., 1996).
58 However, peroxisomes in different organisms host different metabolic pathways and perform
59 diverse functions (Mast et al., 2010). In multicellular organisms, peroxisomes perform both
60 broad and distinct cell-type specific functions; for example, in plants peroxisomes are the sole
61 site for β-oxidation of fatty acids and participate broadly in pathogen defense, however, in
62 stomata they assist in stromal opening, and in mesophyll cells specialized 'leaf' peroxisomes are
63 found tightly juxtaposed to chloroplasts and participate in photorespiration (Kao et al., 2018;
64 Reuman and Weber, 2006). These examples are not exhaustive and peroxisomes perform a
65 variety of other essential and diverse biosynthetic and catabolic processes (Reumann and
66 Bartel, 2016).

67 Peroxisomes respond dramatically to different stimuli. They are induced in metazoans in
68 response to fats, hypolipidemic agents and non-genotoxic carcinogens, and during
69 development and differentiation (Weller et al., 2003). Peroxisome proliferation is linked to their
70 varied functions including, for example, in response to cirrhosis of the liver (De Craemer et al.,
71 1993), after ischemia in the brain (Young et al., 2015), in developing cardiomyocytes (Colasante
72 et al., 2015), in protecting the auditory canal against sound-induced hearing loss from reactive
73 oxygen species (Delmaghani et al., 2015), in epithelial cells to modulate the innate immune
74 system (Dixit et al., 2010; Odendall et al., 2014), in macrophages to assist in clearance of

75 microbial pathogens (Di Cara et al., 2017), and as regulatory sites for the mTOR pathway
76 (Tripathi and Walker, 2016; Zhang et al., 2013; Zhang et al., 2015). In many of these examples,
77 the proliferation of peroxisomes appears to be in response to metabolic need or as part of a
78 stress response to deal with increased levels of harmful molecules, particularly reactive oxygen
79 species, produced through insult or injury. Why this response leads to increased numbers of
80 peroxisomes as opposed to an increase in size is unclear. For example, mice lacking the
81 peroxisome division protein PEX11β have reduced numbers of larger, functional peroxisomes,
82 which does not impede metabolic capacity per se, but yet these mice still display many
83 hallmark phenotypes of peroxisome biogenesis disorder (PBD) patients and die shortly after
84 birth (Li et al., 2002). In contrast, the link between peroxisome proliferation and the role of
85 peroxisomes as spatial beacons for integrating and initiating signaling cascades has become
86 clearer (Mast et al., 2015). Here, changes in peroxisome numbers contribute to tipping the
87 balance between one signaling response versus another, such as in peroxisome-mediated
88 innate immune signaling (Odendall et al., 2014) and regulation of the mTOR pathway (Tripathi
89 and Walker, 2016).
90 Peroxisome proliferation occurs via two partially redundant mechanisms: the division of
91 existing peroxisomes through fission, and de novo formation from the ER (Mast et al., 2015;
92 Smith and Aitchison, 2013). Fission of peroxisomes is comparatively well characterized and
93 requires the Pex11 family of proteins to elongate and constrict the organelle, permitting GTP-
94 dependent scission by dynamin-related proteins (DRPs) (Schrader et al., 2016). Peroxisomes
95 also share division components with other organelles, particularly the mitochondrion (Motley
96 et al., 2008). In contrast, the mechanism of de novo formation remains poorly understood, and

97 the identities of many factors involved in this process remain unknown (Agrawal and
98 Subramani, 2016).

99 In yeast, biogenesis via fission dominates peroxisome proliferation (Motley and
100 Hettema, 2007). However, most peroxisomal membrane proteins (PMPs) transit through the ER
101 on their way to peroxisomes (Hoepfner et al., 2005; Schuldiner et al., 2008; Thoms et al., 2012;
102 van der Zand et al., 2010). A global analysis of localized protein synthesis also revealed that
103 many PMPs are likely cotranslated at the ER (Jan et al., 2014). Similar observations of PMP
104 cotranslation (Kaewsapsak et al., 2017) and transport from ER to peroxisomes made in
105 substantially divergent species of yeast (Agrawal et al., 2011; Farre et al., 2017; Titorenko and
106 Rachubinski, 1998), plants (Hu et al., 2012), the excavate pathogen *Trypanosoma brucei* (Bauer
107 et al., 2017; Guther et al., 2014), and mammalian cells (Kim et al., 2006; Mayerhofer et al.,
108 2016) highlight the essential and evolutionarily ancient role of the ER in peroxisome biogenesis
109 in eukaryotic cells.

110 A vesicular transport pathway transfers proteins and membranes from the ER to
111 peroxisomes (Agrawal et al., 2016; Agrawal et al., 2011; Lam et al., 2010). This pathway is
112 essential even when peroxisomes multiply by growth and division, as altering the flux through
113 this transport pathway alters the numbers of peroxisomes in cells (Mast et al., 2016). Pex3
114 accumulates initially at an ER subdomain before being released in a preperoxisomal vesicle
115 (PPV) that buds from the ER (Halbach et al., 2006; Hoepfner et al., 2005; Tam et al., 2005).
116 Sorting of PMPs through the ER to sites of PPV formation and egress requires both Pex3-
117 dependent and -independent processes (Fakieh et al., 2013). The ER-shaping reticulon proteins,
118 through physical interaction with Pex29 and Pex30, assist in regulating Pex3 sorting through the

119 ER and releasing PPVs (David et al., 2013; Mast et al., 2016). Pex30 and its paralogue, Pex31,
120 have membrane-shaping capabilities like the reticulon proteins, which may help in defining and
121 segregating the PPV exit site in the ER (Joshi et al., 2016).

122 The formation of PPVs requires Pex3 and Pex19, and loss of PPV formation leads to a
123 cell's inability to form peroxisomes and consequently its eventual loss of the organelle
124 (Hettema et al., 2000; Hoepfner et al., 2005). Pex19 is a cytosolic protein that interacts with
125 Pex3 and other PMPs (Agrawal et al., 2017), functioning as a chaperone, and is essential for
126 budding PPVs from the ER (Lam et al., 2010). At least two classes of PPVs (V1 and V2) have been
127 characterized (Agrawal et al., 2016; Titorenko et al., 2000; Titorenko and Rachubinski, 2000; van
128 der Zand et al., 2012); both contain Pex3 but differ in whether they contain or lack docking-
129 factor or RING finger group proteins of the peroxisomal matrix protein import complex
130 (peroxisomal importomer) (Agrawal et al., 2016). The separation of these two subcomplexes
131 could prevent premature assembly of the peroxisomal importomer in the ER and the potential
132 import of peroxisomal matrix proteins directly into the ER (Agrawal et al., 2016; van der Zand et
133 al., 2012). While Pex3 and Pex19 are necessary for PPV budding, they are not sufficient for this
134 process, and evidence suggests additional cytosolic component(s) are required, at least one of
135 which likely consumes ATP (Agrawal et al., 2011; Lam et al., 2010). DRPs, which function in
136 peroxisome division, or COPI and COPII vesicle transport pathways, all of which consume GTP,
137 have repeatedly been shown not to be required for PPV formation (Lam et al., 2010; Motley et
138 al., 2015; Motley and Hettema, 2007; Perry et al., 2009; South et al., 2000).

139 Here, we report a novel role for endosomal sorting complexes required for transport
140 (ESCRT)-III in the de novo biogenesis of peroxisomes. In particular, using a series of

141 comprehensive morphological and genetic assays of peroxisome formation and function and in
142 vitro biochemical assays that produce PPVs from the ER, we implicate ESCRT-III as being
143 essential for the scission of PPVs from the ER.

144 Results

145 Genomic screens identify a putative role for ESCRT in peroxisome biogenesis

146 Screens of an isogenic, arrayed collection of yeast gene deletion strains identified 211 genes
147 whose disruption led to defects in the cell's ability to form peroxisomes (Saleem et al., 2010).
148 We reasoned that this dataset held clues to candidates involved in the de novo biogenesis of
149 peroxisomes and in the formation of PPVs at the ER. Candidates would be expected a priori to
150 be cytosolic and/or localized to the ER, and to use ATP in their activity. Components of ESCRT
151 exhibit these characteristics and were enriched in this dataset with a statistically significant
152 hypergeometric p-value of 0.003 (Saleem et al., 2010).

153 ESCRT is composed of five subcomplexes, including ESCRT-0, -I, -II, -III (and -III-
154 associated), and the AAA-ATPase Vps4 complex (Babst et al., 2002a; Babst et al., 2002b; Babst
155 et al., 1997; Katzmann et al., 2001; Katzmann et al., 2003) (reviewed in (Henne et al., 2011;
156 Schoneberg et al., 2016)). These five complexes function sequentially to mediate the formation
157 of intraluminal vesicles and also assist in piecemeal fashion in numerous other cellular activities
158 like cytokinesis (Carlton and Martin-Serrano, 2007), plasma membrane repair (Jimenez et al.,
159 2014; Scheffer et al., 2014), autophagosome closure (Lee et al., 2007; Rusten et al., 2007), viral
160 replication and budding (Garrus et al., 2001), nuclear envelope reformation (Olmos et al., 2015;
161 Vietri et al., 2015), nuclear pore complex quality surveillance (Webster et al., 2014), neuronal
162 pruning (Loncle et al., 2015), and microtubule severing (Guizetti et al., 2011) (Henne et al.,

163 2011; Schoneberg et al., 2016). ESCRT-III, composed of Vps20, Snf7, Vps24 and Did4 in yeast, is
164 evolutionarily ancient and is the primary effector complex for all these activities (Henne et al.,
165 2011; Tang et al., 2015). Given this wealth of function, particularly for ESCRT-III, a key
166 consideration was whether ESCRTs have a direct role in peroxisome biogenesis or exert indirect
167 effects due to their diversity of activity. In our global screens for peroxisome effectors (Saleem
168 et al., 2010; Smith et al., 2006), ESCRT deletion strains showed defects in metabolizing fatty acid
169 carbon sources, a process requiring functional peroxisomes; had altered expression of the
170 peroxisomal β-oxidation enzyme 3-ketoacyl-CoA thiolase (Pot1); but exhibited only mild or no
171 peroxisome morphology defects as assessed by high-throughput fluorescence microscopy
172 (Table S1).

173 **Yeast strains lacking ESCRT-III components exhibit oleic acid-specific growth defects**

174 We used our one-cell doubling evaluation of living arrays of yeast (ODELAY!) platform (Herricks
175 et al., 2017a) to re-address the role of ESCRT in peroxisome biogenesis by comparing growth on
176 solid-phase medium containing as the sole carbon source either glucose or oleic acid, which
177 requires functional peroxisomes for its metabolism (Figs. 1 and S1). Unlike traditional spot-
178 based assays or assays using optical density measurements at a population level, ODELAY!
179 provides time-resolved measurements of yeast populations growing from individual cells into
180 colonies, for an array of up to 96 different strains (Herricks et al., 2017a). ODELAY! therefore
181 permits standardized analyses of the growth rates and population heterogeneity both within
182 and between strains measured in parallel across different growth conditions. Strains with
183 general growth defects have comparable normalized growth rates under both conditions,
184 whereas condition-specific strains grow more slowly under one condition versus another. We

185 measured growth rates for all 18 ESCRT deletion strains, 6 peroxin/peroxisome-related control
186 deletion strains, and 20 randomly selected deletion strains from the yeast deletion library (Fig.
187 1 A and Table S2).

188 Strain doubling times measured by ODELAY! were normalized, and the mean *Z*-score for
189 each deletion strain was compared between the two growth conditions (Fig. 1 A). The *pex19*Δ,
190 *pex13*Δ and *pex14*Δ strains, which lack the ability to form peroxisomes (Hettema et al., 2000)
191 and a functional peroxisomal importomer (Meinecke et al., 2010), or the *pot1*Δ strain lacking
192 the enzyme that performs the last step of peroxisomal β-oxidation (Igual et al., 1991), revealed
193 condition-specific growth defects, as they exhibited slightly faster or marginally slower growth
194 in the presence of glucose but grew 4-5 standard deviations more slowly than the
195 corresponding wild-type strain *BY4742* in the presence of oleic acid (Fig. 1 A).

196 ESCRT-III deletion strains showed pronounced condition-specific growth defects in the
197 presence of oleic acid, with *did4*Δ cells registering the slowest doubling rate of all ESCRT
198 deletions, followed by *vps20*Δ, *snf7*Δ and *ist1*Δ, which is a deletion strain for an ESCRT-III
199 associated gene (Fig. 1 A). ESCRT-I deletion strains displayed general growth defects, whereas
200 ESCRT-II deletion strains clustered tightly, in line with their known structural and functional
201 assembly as a single protein complex, and showed a condition-specific growth defect in oleic
202 acid, although not as severe as that observed for strains deleted for ESCRT-III components (Fig.
203 1 A). Other ESCRT deletion strains also had slower, but less severe, doubling times in oleic acid
204 than ESCRT-III deletion strains, except for the strain lacking the Vps4 regulator Vta1 which, like
205 the peroxisome inheritance mutants *inp1*Δ and *inp2*Δ, had a faster doubling time than the wild-
206 type strain under both glucose and oleic acid conditions (Fig. 1 A).

207 Despite the skew to oleic acid-specific growth defects observed for the majority of
208 ESCRT deletion strains in the *BY4742* background, the randomly selected gene deletions
209 revealed no bias in our assay (Fig. 1 A and Table S2). Of note, *sec28*Δ, a strain lacking the ε-COP
210 subunit of coatomer (Duden et al., 1998), demonstrated a significant growth defect when
211 grown on medium containing glucose but grew significantly faster than the wild-type strain on
212 medium containing oleic acid (Fig. 1 A and Table S2). This phenotype could partially result from
213 the overall slower growth of cells metabolizing oleic acid, which would mask defects in COPI
214 vesicle trafficking, and also further demonstrates that COPI is not involved in peroxisome
215 biogenesis. Other deletion strains affecting the secretory pathway, such as *emp46*Δ, lacking a
216 COPII-associated protein (Sato and Nakano, 2002), or *nyv1*Δ, lacking a v-SNARE of the vacuolar
217 SNARE complex (Nichols et al., 1997), showed negligible general growth defects (Fig. 1 A and
218 Table S2). Therefore, general defects in endocytic trafficking do not manifest as condition-
219 specific defects in the metabolism of the non-fermentable carbon source, oleic acid.

220 We repeated our ODELAY! analysis in the *W303* strain background and evaluated strains
221 deleted for the genes *VPS20*, *SNF7*, *DID4* and *VPS24* encoding ESCRT-III components, together
222 with strains deleted for the genes *IST1* and *VPS25* (Fig. 1 B and Table S2). We observed similar
223 condition-specific growth defects for the ESCRT-III deletion strains in the presence of oleic acid
224 in the *W303* strain background as we had observed in the *BY4742* strain background (Fig. 1 A
225 and Table S2) However, for *vps25*Δ, while oleic acid-specific defects were observed in the
226 *BY4742* strain deleted for *VPS25* (Fig. 1 A), these condition-specific defects were not
227 reproduced in the *W303* strain deleted for *VPS25*, which displayed general and equivalent
228 growth defects on both glucose and oleic acid carbon sources (Fig. 1 B). The *ist1*Δ strain, which

229 showed condition-specific growth defects in *BY4742*, showed negligible growth defects in
230 *W303*, where it grew faster than *wild-type* in the presence of glucose and slightly slower than
231 *wild-type* in the presence of oleic acid (Fig. 1 B). We therefore conclude that ESCRT-III has a
232 specific functional role in the metabolism of the non-fermentable carbon source, oleic acid.

233 **Loss of ESCRT-III components results in peroxisomes with aberrant morphologies**

234 To determine if the growth defects observed for ESCRT-III mutants result from defects in
235 peroxisomes, we used EM to investigate the cellular ultrastructure of cells lacking individual
236 components of the core ESCRT-III complex under conditions that promote peroxisome
237 biogenesis (Figs. 2 and S1). Yeast were grown in the presence of oleic acid for 8 h to induce
238 peroxisome proliferation and peroxisomal membrane expansion (Saleem et al., 2008; Smith et
239 al., 2002). Under these conditions peroxisomes were readily observed in *wild-type* cells as
240 orbicular structures delimited by a single lipid bilayer and containing an electron-dense,
241 paracrystalline matrix (Fig. 2 A). In contrast, peroxisomes were not observed in *vps20Δ* or *snf7*Δ
242 cells, which instead contained infrequent small vesicular structures of unknown origin, although
243 often in close apposition to, and possibly contiguous with, ER membranes (Fig. 2, B and C).
244 Quantification revealed fewer peroxisomes and vesicular-like structures for all deletion strains
245 of the ESCRT-III complex (Fig. 2 D and Table 1), although peroxisomes similar in size to *wild-type*
246 peroxisomes were observed in *did4*Δ and *vps24*Δ cells, but at levels 25% and 45%, respectively,
247 of peroxisomes in *wild-type* cells (Fig. 2, E - I).

248 **ESCRT-III components act as positive effectors of de novo peroxisome assembly**

249 The observed growth and peroxisome morphology defects detected for deletion strains of
250 ESCRT-III and in particular for *vps20*Δ and *snf7*Δ mutants suggested a role for ESCRT-III in

251 peroxisome biogenesis. To test this, we used an in vivo peroxisome biogenesis assay in which
252 tetracycline control of *PEX19* expression permits synchronization of cells for de novo
253 peroxisome biogenesis without overexpressing peroxins (Fig. 3 A) (Mast et al., 2016). This is a
254 critical distinction from de novo biogenesis assays that rely on repression and then
255 overexpression of a peroxin, as it does not lead to mistargeting of the peroxisomal reporter to
256 the general ER or other organelles. With *PEX19* expressed, *wild-type* cells contained an average
257 of 10 peroxisomes per cell, as assessed by the punctate localization of peroxisomal Gpd1-GFP
258 (Fig. 3 A) (Jung et al., 2010). Repression of *PEX19* expression by treatment with doxycycline
259 (DOX) for 24 h removed peroxisomes from the *wild-type* yeast population, with only ~0.2% of
260 cells containing on average one peroxisome per cell. Removal of DOX enabled the expression of
261 *PEX19* and initiated de novo biogenesis of peroxisomes (Fig. 3 A). We tracked peroxisome
262 formation using three-dimensional fluorescence microscopy over 24 h, sampling cells at 0, 4, 8,
263 12 and 24 h after initiation of de novo peroxisome biogenesis. Quantification of the number of
264 peroxisomes per cell revealed a population distribution of steady-state peroxisome densities
265 comparable to those we have measured previously (Fig. 3 B) (Mast et al., 2016).
266 The assembly of peroxisomes de novo is a dynamical systems process that proceeds
267 non-linearly following reintroduction of *PEX19* (Fig. 3). In *wild-type* cells, peroxisomes
268 reappeared in 91% of cells 4 h after induction of *PEX19* and proceeded to overshoot steady-
269 state levels of peroxisomes 8 h post-induction. By 12 h, the population distribution of
270 peroxisome levels had dropped below those at steady-state, and by 24 h were still on a
271 trajectory to return to steady-state levels. The dynamics of de novo peroxisome formation were
272 strongly influenced by the length of repression of *PEX19* and by the state of cell growth, in

273 accordance with our previous observations (Mast et al., 2016). These current observations
274 imply the existence of positive and negative regulators of de novo peroxisome biogenesis.
275 Strikingly, ESCRT-III mutants displayed severe defects in de novo peroxisome biogenesis.
276 ESCRT-III mutants had fewer peroxisomes per cell under steady-state conditions and retained
277 more peroxisomes per cell following DOX repression of *PEX19* (Fig. 3). Upon stimulation of de
278 novo peroxisome biogenesis, *vps20*Δ, *snf7*Δ, *did*4Δ and *vps24*Δ cells, in order of severity, failed
279 to produce peroxisomes at rates comparable to that of *wild-type* cells, revealing a defect in the
280 ability of *vps20*Δ and *snf7*Δ cells especially to form new peroxisomes de novo (Fig. 3).
281 Pex19 dynamics in *wild-type* cells presaged peroxisome dynamics in these cells, as Pex19
282 levels returned to steady-state 4 h after release of DOX-induced repression, then leveled off
283 and dropped slightly at 8 and 12 h, before increasing slightly at 24 h post-induction (Fig. 4). Like
284 *wild-type*, ESCRT-III mutants showed no detectable levels of Pex19 following DOX treatment,
285 but by 4h post-induction Pex19 levels were comparable to those found in *wild-type* cells.
286 However, Pex19 dynamics were altered in the ESCRT-III mutants as compared to *wild-type* (Fig.
287 4). We conclude that while Pex19 dynamics were altered in ESCRT-III mutants, ESCRT-III
288 mutants nonetheless expressed sufficient Pex19 at all times following removal of DOX to rule
289 out a contribution of altered Pex19 dynamics as the primary explanation for the catastrophic de
290 novo biogenesis defects observed in these strains.

291 **ESCRT-III functions conditionally downstream of Pex19**

292 The interplay between Pex19 dynamics and peroxisome dynamics and the interruption of that
293 interplay in ESCRT-III mutants suggested to us the potential for genetic interactions between
294 Pex19 and ESCRT-III. Genetic interactions can often provide insights into the function of

295 proteins, order pathways, and reveal coordinated functions (Costanzo et al., 2016; Schuldiner et
296 al., 2005). Common examples of genetic interactions include epistasis, where two mutants have
297 phenotypes different from that of *wild-type* and the double mutant shows the phenotype of
298 one of the single mutants. These "alleviating" interactions suggest that one protein functions
299 upstream of the other in a linear pathway (Mani et al., 2008). Similarly, synthesis occurs when
300 the phenotype of a double mutant is more severe than an additive effect of the individual
301 mutant phenotypes. Common interpretations of this scenario include proteins that function in
302 parallel biological pathways or form structures that cannot withstand, or 'buffer', the loss of
303 both components (Dixon et al., 2009). More complex modes of genetic interaction also exist,
304 including single-nonmonotonic, where a single mutant shows opposing phenotypes in the *wild-*
305 *type* and other single mutant backgrounds (Drees et al., 2005). There are no common
306 interpretations for this scenario, but such an interaction would imply that epistasis exists under
307 a limiting set of circumstances.

308 Using ODELAY!, we measured growth rates for the tetracycline-regulated *PEX19*
309 background strain as well as strains additionally harboring ESCRT-III deletion mutants under
310 conditions where *PEX19* was differentially expressed. The normalized mean *Z*-scores were
311 plotted on a phenotypic axis for each ESCRT-III mutant alongside its corresponding phenotype
312 (Φ) inequalities (Fig. 5) (Drees et al., 2005). This unbiased and quantitative analysis revealed
313 complex genetic interactions between *PEX19* and ESCRT-III with *did4*Δ, *vps20*Δ and, to a lesser
314 extent, *snf7*Δ being single-nonmonotonic to *PEX19* depletion. Whereas *vps24*Δ, and potentially
315 *snf7*Δ, is epistatic to *PEX19* depletion, *ist1*Δ is double-nonmonotonic with *PEX19* depletion. We
316 interpret these results to suggest that ESCRT-III functions conditionally downstream of *PEX19*,

317 i.e. the function of ESCRT-III is contextual and specific to the budding of peroxisomes from the
318 ER.

319 Notably, ESCRT-III localized to sites of de novo peroxisome biogenesis. As expected,
320 Pex3-GFP and Snf7-mCherry puncta rarely overlapped under steady-state control conditions,
321 but 13.5% of Pex3p-GFP puncta correspondingly colocalized with the Snf7-mCherry signal
322 following release from DOX treatment to induce de novo peroxisome formation (Fig. 6 A).
323 Interestingly, Pex3-GFP foci colocalizing with Snf7-mCherry were dimmer and sometimes
324 elongated, similar in appearance to previous observations of Pex3 in cells repressed for
325 members of the *DSL1* protein complex (Perry et al., 2009) and for Pex3 that colocalized with
326 Pex30 and Pex29 in the ER under steady-state conditions (Mast et al., 2016). We were unable to
327 detect a meaningful fluorescence signal for Vps20-mCherry and Vps24-mCherry under these
328 conditions; however, Did4-mCherry showed a pattern similar to that of Snf7-mCherry despite
329 having a very low signal-to-noise ratio (Fig. 6 B). The reduction in colocalization of Did4-
330 mCherry compared to Snf7-mCherry may be biologically relevant or may reflect the low
331 fluorescence signal for Did4-mCherry that was measured for these cells.

332 **ESCRT-III is required for the release of preperoxisomal vesicles from the ER**

333 Current models of ESCRT-III function propose that Vps20 is recruited to a membrane first,
334 initiating activation and polymerization of additional members, especially Snf7, to form spirals
335 and coils that deform membranes into tubes or cones to achieve membrane scission (Henne et
336 al., 2011; Schoneberg et al., 2016). Vps24 caps the polymers and stops polymerization, whereas
337 Did4 is integrated into the polymer to promote its disassembly by recruiting the AAA-ATPase,
338 Vps4 (Henne et al., 2011; Schoneberg et al., 2016).

339 We used an in vitro budding assay that reconstitutes the packaging and release of PMPs
340 from the ER via PPVs (Lam et al., 2010, Mast et al., 2016) to test if ESCRT-III is required for PPV
341 scission at the ER (Fig. 7). ER membranes were prepared from a *pex19*Δ strain in which Pex3
342 and other PMPs are trapped in the ER (Agrawal et al., 2016; Agrawal et al., 2011). The release of
343 Pex3 was stimulated by addition of *wild-type* cytosol and an ATP regeneration system (Lam et
344 al., 2010) but not by cytosol from *pex19*Δ, *vps20*Δ, or *snf7*Δ cells (Fig. 7 A and C). We also tested
345 cytosols from other ESCRT and ESCRT-III deletion strains, e.g. *did4*Δ and *vps24*Δ, and found that
346 their cytosols still promoted the formation of Pex3-containing PPVs but sometimes at levels
347 significantly less than that produced by *wild-type* cytosol (Figs. 7 A and S2). Defects in budding
348 were independent of the levels of Pex19 in ESCRT-III mutant strains (Fig. S3). The defect in PPV
349 budding was also independent of the background yeast strain, as similar results were obtained
350 using cytosols obtained from deletion strains in the *W303* strain background (Fig. 7 B). Mixing
351 the 100 k*g* supernatant fraction of cytosols (S100) from *snf7*Δ, *vps20Δ* and *pex19Δ* strains
352 pairwise in a 1:1 ratio complemented the defect in Pex3 release (Fig. 7, C and D).
353 Complementation was also achieved by expressing exogenous copies of *VPS20* or *SNF7* in their
354 respective deletion strains (Fig. 7, E and F). Here, the likely overexpression of *VPS20* led to
355 enhanced PPV release, whereas the likely overexpression of *SNF7* did not. The production of
356 PPVs at 4 °C suggested that scission is mechanical and not reliant on ATP-dependent enzymatic
357 activity (Fig. 7 A – D). It is known that ESCRT-III does not depend on ATP hydrolysis to mediate
358 membrane scission but rather relies on the AAA-ATPase Vps4 to remove and recycle ESCRT-III
359 components (Wollert et al., 2009). Accordingly, treatment of the reaction with apyrase to
360 deplete ATP led to a reduction, but not abrogation, of PPV budding that could be restored to

361 typical levels by addition of exogenous ATP (Fig. 7 G). Consistent with this observation, PPV
362 release occurred rapidly upon reaction mixing, followed by further incremental release over
363 time, suggesting that ATP acts primarily in recycling scission components (Fig. 7 G).

364 Discussion

365 ESCRT-III components, particularly Vps20 and Snf7, can be envisaged as "peroxins", as they are
366 required for peroxisomal membrane biogenesis and peroxisome proliferation (Distel et al.,
367 1996). Here, we demonstrated that ESCRT-III deletion mutants have condition-specific growth
368 defects when grown on a non-fermentable carbon source, oleic acid (Fig. 1), the metabolism of
369 which requires functional peroxisomes. We show that morphologically identifiable peroxisomes
370 are absent in *vps20*Δ and *snf7*Δ cells by EM, while *did4*Δ and *vps24*Δ cells have drastically
371 reduced numbers of peroxisomes (Fig. 2). Our experiments revealed that ESCRT-III components
372 act as positive effectors of de novo peroxisome biogenesis, as their absence leads to fewer
373 numbers of peroxisomes at steady-state and inhibits de novo peroxisome formation, and
374 because they function downstream of Pex19 in this process as assessed by genetic interactions
375 (Figs. 3 and 5). The ESCRT-III proteins Snf7 and Did4 dynamically localize to sites of de novo
376 peroxisome biogenesis (Fig. 6), and in cell-free experiments Vps20 and Snf7 are required for the
377 release of Pex3-containing PPVs from the ER (Fig. 7).

378 In the genome-wide screens that led us to ESCRT-III and its role in de novo peroxisome
379 biogenesis, and in our experiments here (Fig. 3), import-competent peroxisomes can be found
380 at steady-state levels in ESCRT-III deletion mutants. How can this observation be reconciled
381 with a role for ESCRT-III in scissioning PPVs from the ER? In the case of COPI and COPII, vesicle
382 scission can occur independently of GTP hydrolysis by simply requiring the assembly of fission-

383 competent coated vesicles for fission to occur (Adolf et al., 2013). Thus, it is conceivable that a
384 small proportion of budded PPVs, arrested in a fission-competent state, could be released from
385 the ER stochastically. Following vesicle release and carrying the full complement of peroxins
386 necessary for PPV maturation, these PPVs would become mature peroxisomes, and the growth
387 and division cycle of peroxisome biogenesis could thereafter sustain the peroxisome
388 population. Furthermore, as demonstrated for peroxisome fission (Motley and Hettema, 2007),
389 we also cannot exclude a role for peroxisome inheritance factors in partially compensating for
390 the loss of ESCRT-III. Inp2 is a membrane protein and the receptor for the motor Myo2 that
391 actively transports peroxisomes from mother cell to bud (Fagarasanu et al., 2006; Fagarasanu et
392 al., 2009). The presence of Inp2 in a budded vesicle at the ER could be envisaged to be sufficient
393 to physically pull PPVs off the ER. Consistent with such a scenario is recent evidence showing
394 preferential Inp2-directed inheritance of young peroxisomes to growing daughter cells (Kumar
395 et al., 2017). Notwithstanding these possibilities, it is clear that peroxisomes in ESCRT-III
396 mutants, although import-competent, are nevertheless aberrant and non-functional (Figs. 1, 2
397 and 3).

398 The formation of PPVs shares features and characteristics that are fundamental to all
399 vesicle biogenesis events. These include cargo protein sorting and trafficking to sites of vesicle
400 formation, the presence of adaptor molecules to guide cargo sorting and to remodel the
401 membrane to form a budding vesicle, and scission machinery to release the vesicle to the
402 cytosol (Spang, 2008). However, there are also fundamental differences between classical
403 vesicle biogenesis and PPV biogenesis. Unlike the vesicles of the secretory pathway, PPVs are
404 not coated (Titorenko and Rachubinski, 1998). PPVs also do not carry cargo in their matrix and,

405 although it is still unknown how, must exclude components of the ER matrix. PPVs therefore
406 share similarities with nascent lipid droplets, and similarities in PPV and lipid droplet formation,
407 as well as shared components guiding their biogenesis, have recently come to light (Schrul and
408 Kopito, 2016; Schuldiner and Bohnert, 2017).

409 Our observations are consistent with a model wherein Vps20 is recruited to sites of PPV
410 formation, which in turn recruits and activates the polymerization of Snf7 to drive membrane
411 scission and release of the PPV to the cytosol. Other ESCRT-III proteins like Did4 and Vps24 are
412 also involved in PPV scission but are not essential for this process, and probably influence the
413 dynamics of PPV formation and recruit the machinery for disassembly of ESCRT-III at the ER.
414 Consistent with such a scenario, the *did4*Δ strain displayed severe growth defects in the
415 presence of oleic acid and showed reduced budding of Pex3-positive PPVs from the ER (Figs. 1
416 and 7). Both *did4*Δ and *vps24*Δ cells showed delays in de novo peroxisome biogenesis in vivo
417 (Fig. 3). This observation is consistent with a role for Did4 and Vps24 in recruiting the AAA-
418 ATPase Vps4 complex to disassemble ESCRT-III polymers and with previous observations that
419 the amount of cytosolic Snf7 is reduced in *did4*Δ cells because it is trapped in a polymerized
420 state on membranes (Babst et al., 2002a). However, our observations may also reflect a more
421 fundamental role for Vps24 and particularly Did4 in shaping the overall topology of the ESCRT-
422 III polymer to be suitable for PPV scission.

423 ESCRT-III is typically thought to be involved in vesicle budding *away from* the cytosol
424 (reverse-topology membrane scission) with or without other ESCRT complexes (subsets of
425 ESCRT-0, -I and -II) (Henne et al., 2011; Schoneberg et al., 2016). Our data extend ESCRT-III
426 function to include vesicle budding *into* the cytosol (normal-topology membrane scission).

427 Consistent with our hypothesis, cryo-EM images of purified ESCRT-III components
428 demonstrated that ESCRT-III can deform and stabilize membranes for normal-topology scission
429 (McCullough et al., 2015). While normal-topology membrane scission required mammalian
430 *IST1*, our observations rule out a similar role for Ist1 in peroxisome biogenesis, and instead
431 suggest that it is the core ESCRT-III components that are capable of normal-topology membrane
432 scission in regard to PPV biogenesis in yeast (Fig. 7). However, there may be species-specific
433 differences in regard to ESCRT-III function in de novo peroxisome biogenesis, and it will be
434 important to test the role of ESCRT-III in peroxisome biogenesis in other organisms. At this
435 time, we also cannot rule out the possibility that ESCRT-III release of PPVs from the ER proceeds
436 as a reverse-topology scission event. In this hypothetical scenario, dense tubulated matrices of
437 ER (Nixon-Abell et al., 2016) would serve as a template for ESCRT-III to assemble as a ring
438 through which a budded PPV could pass and be cleaved. Understanding the molecular
439 mechanisms of ESCRT-III function in de novo peroxisome biogenesis in greater detail is
440 undoubtedly a high priority for future research.
441 ESCRT-III has been implicated in unconventional protein secretion from the ER with its
442 mode of action unclear (Curwin et al., 2016). It is interesting to note that unconventional
443 protein secretion has previously been linked to peroxisomes (Manjithaya et al., 2010), and may
444 more broadly share a common mechanism of egress with PPVs from the ER. Peroxisomes and
445 ESCRT-III have also been implicated in prospore membrane formation, which requires a supply
446 of vesicles to be delivered to and to fuse with the growing prospore membrane (Briza et al.,
447 2002). Rather than attribute a putative metabolic role for peroxisomes in these processes, it is
448 plausible that the non-classical vesicle secretion pathway that gives rise to peroxisomes, reliant

449 on peroxins and ESCRT-III, is a general non-coated secretion pathway that is used more broadly
450 by cells. The expanding role of ESCRT-III in diverse cellular activities, including the formation of
451 peroxisomes, suggests that this evolutionarily ancient protein complex has had a much greater
452 influence on sculpting the eukaryotic bauplan than previously realized.

453 Materials and methods

454 Yeast strains and plasmids

455 The yeast strains used in this study are listed in Table S3 and were derived from the parental
456 strain *BY4742* or the corresponding gene deletion strain library (Invitrogen) (Giaever et al.,
457 2002), the parental strain *W303a* (Rothstein et al., 1977), or the parental strain *R1158*
458 (Mnaimneh et al., 2004), as described previously (Mast et al., 2016). Strains harboring genomic
459 insertions and deletions were isolated following homologous recombination with targeted PCR
460 fragments delivered via chemical transformation. Correct integration was verified by PCR across
461 junctions using gene-specific primers. The following plasmids were used for PCR amplification
462 with appropriate primers as described: pGFP/*SpHIS5* (Dilworth et al., 2001); pProtA/*SpHIS5*
463 (Aitchison et al., 1995); pCM189/*URA3* (Gari et al., 1997); pBS34/*hph* (mCherry) (Shaner et al.,
464 2004); and pFA6a-*nat*NT2 and pFA6a-*hph*NT1 (Janke et al., 2004). pCM189-*VPS20* was
465 assembled by cloning a 666-bp BamHI/NotI fragment encoding full-length *VPS20* into pCM189.
466 pCM189-*SNF7* was assembled by cloning a 723-bp BamHI/NotI fragment encoding full-length
467 *SNF7* into pCM189.

468 Yeast media and growth conditions

469 Yeast strains were grown in YPD medium (1% yeast extract, 2% peptone, 2% glucose) or YPBO
470 medium (0.5% KP_i, pH 6.0, 0.3% yeast extract, 0.5% peptone, 0.5 % Tween 40, 0.15% oleic acid),
471 as indicated. All cultures were grown at 30°C. When marker selection was required, defined
472 synthetic medium (SM) supplemented with 2% glucose and the necessary amino acid(s) or drug
473 was used. Yeast media and growth conditions for specific experiments are listed below.
474 YPB-oleate medium for use in ODELAY! was prepared as follows. A solution of 300 mg of
475 methyl-β-cyclodextrin (Sigma)/mL and 10 µL oleic acid/mL was prepared in absolute ethanol for
476 a total volume of 3 mL. The solution was then placed in a Rotovap for 3 h to remove the
477 ethanol. The resulting powder was then reconstituted using ultra-pure H_2O to a total volume of
478 3 mL. Meanwhile 15 mL of 1.33% agarose, 2 mL of 10 × YPB medium, and 1 mL of ultra-pure
479 H_2O were melted in boiling water for 18 min. Then 2 mL of the oleate-cyclodextrin solution
480 were added to the melted medium and vortexed to mix. The YPB-oleate medium was then cast
481 into molds and allowed to cool as described (Herricks et al., 2017a). YPB-glucose medium was
482 prepared similarly except 2 mL of 20% glucose were added instead of the oleate-carbon source.
483 To study peroxisome biogenesis, strains were grown overnight to saturation in YPD medium
484 and diluted the next morning by dilution into fresh YPD medium to an OD_{600} = 0.2. Cells were
485 then allowed to reach logarithmic phase (OD_{600} = 0.7-1) before being diluted again in YPD
486 medium, supplemented with 4 µM DOX, and incubated for 24 h. The logarithmic phase cells
487 were harvested by centrifugation, washed five times in YPD medium to remove DOX, inoculated
488 into fresh YPD medium without DOX at an OD_{600} = 0.2, and cultured for an additional 24 h. At 4,
489 8, and 12 h, OD_{600} measurements were taken, and cultures were diluted as necessary to
490 maintain logarithmic growth. Localization of ESCRT-III components to sites of peroxisome

491 biogenesis used a similar growth scheme, but was performed in YPD medium containing 2 µM
492 DOX and for 18 h.

493 **One-cell doubling evaluation of living arrays of yeast (ODELAY!)**

494 Sensitive, high-density, and multiparametric analysis of cell growth was performed as described
495 (Herricks et al., 2017a; Herricks et al., 2017b). Briefly, yeast was cultured in YPD medium in 96
496 well plates at 30˚C overnight. Cultures were diluted to an OD_{600} = 0.09 and allowed to grow for
497 6 h at 30˚C. The cultures were then washed in YPB medium without a carbon source, diluted to
498 an OD_{600} = 0.02, and spotted onto YBP-oleate or YPB-glucose agarose medium. The resulting
499 cultures were then observed using time-lapse microscopy for 48 h with 30 min intervals
500 between images. All images were collected on a Leica DMI6000 microscope equipped with a
501 10× 0.3 NA lens using bright field microscopy. MATLAB scripts using the Micro-Manager
502 interface controlled the image collection process (Edelstein et al., 2014).

503 Population growth rates were scored against each other using the equation:

$$Z_{mean} = \frac{1}{n}\sum_{i}^{n}\frac{d_i - \mu_i}{\sigma_i}$$

504 Where d_i is the *i*th decile of query population doubling time, μ_i is the mean of the *i*th decile of
505 the parental strain's doubling time, and σ_i is the standard deviation of the *i*th decile of the
506 parental strain's doubling time. The mean and standard deviation deciles (μ_i and σ_i) were
507 calculated from 16 separate *wild-type* and 8 separate deletion strain populations containing at
508 least 200 individuals per replicate. All calculations were performed using MATLAB scripts
509 (Herricks et al., 2017a).

510 **EM and quantification**

511 Experiments were performed as described (Tam et al., 2003). Strains were cultured in YPBO
512 medium for 8 h before being fixed and processed for EM. Image analysis to measure cell and
513 peroxisome profiles was performed in Image J (National Institutes of Health). Stereological
514 analysis to derive numerical densities of peroxisomes was performed as described (Weibel and
515 Bolender, 1973).

516 **Fluorescence microscopy and quantification**

517 Experiments were performed as described (Mast et al., 2016). Briefly, 10 fields of view yielding
518 at least 100 cells per strain per time point for Gpd1-GFP labeled cells and at least 75 cells per
519 strain per time point for Pex3-GFP/Snf7-mCherry-labeled cells or Pex3-GFP/Did4-mCherry-
520 labeled cells were acquired in a semi-automated and randomized fashion with bright field or
521 calcofluor white staining used to establish focus for each strain and time point. Images were
522 acquired with a 100× 1.4 NA objective (Olympus) on a DeltaVision Elite High Resolution
523 Microscope (GE Healthcare Life Sciences). Images were deconvolved with the manufacturer's
524 supplied deconvolution software (softWoRx) and an experimentally determined point spread
525 function. Images were further processed using Imaris software (Bitplane), and object-based
526 colocalization analysis (Bolte and Cordelieres, 2006) was performed using the "Spots" function
527 as described previously (Mast et al., 2016). Experiments were performed in triplicate.

528 **Preparation of yeast whole cell lysates**

529 Yeast whole cell lysates were prepared by denaturation in alkali solution with a reducing agent.
530 Approximately 1.85×10^8 cells (5 OD_{600} cell units) were harvested by centrifugation at $5{,}000 \times g$

531 for 2 min, and resuspended in 240 µL of 1.85 M NaOH to which 7.4% (v/v) of 2-
532 mercaptoethanol had been freshly added. The cell suspension was incubated on ice for 5 min
533 and then mixed with an equal volume of 50% TCA by vortexing. After a 5 min incubation on ice,
534 the precipitated protein was collected by centrifugation at 16,000 × *g* for 10 min at 4˚C. The
535 pellet was washed once with ice-cold water and resuspended in 50 µL of Magic A (1 M
536 unbuffered Tris-HCl, 13% SDS) to which 50 µL of Magic B (30% glycerol, 200 mM DTT, 0.25%
537 bromophenol blue) were added.

538 **Antibodies and antisera**

539 Antibodies to GFP (Sigma), pA-affinity purified rabbit IgG (Mast et al., 2016), and antiserum to
540 Kar2 (Tam et al., 2005) have been described. Antiserum to Pex19 was raised in guinea pig
541 against full-length Pex19 lacking the carboxyl-terminal CKQQ farnesylation motif. $Pex19^{1-338}$ was
542 expressed as a fusion protein to glutathione-S-transferase (PEX19-GST), purified from
543 *Escherichia coli* lysate on anti-GST Sepharose, liberated by cleavage with thrombin (removed by
544 addition of benzamidine Sepharose), and concentrated using an Amicon Ultra centrifugal filter.
545 Antiserum was tested for specificity for Pex19 by immunoblot of whole cell lysates from *wild-*
546 *type*, *pex19*Δ, and *PEX19-pA* strains.

547 **In vitro PPV budding assay**

548 Experiments were performed as described (Mast et al., 2016). Permeabilized yeast cells were
549 prepared from *pex19*Δ cells expressing Pex3-pA or Pex3-GFP from an endogenous promoter.
550 Cells were grown overnight in 1 L of YPD medium to an OD_{600} of 1. Cells were collected by
551 centrifugation at 2,000 × *g* for 7 min at room temperature, resuspended in low glucose medium

552 (YPD medium containing 0.1% glucose), and incubated for 30 min at 25°C with vigorous shaking.
553 Cells were harvested by centrifugation and resuspended in spheroplast medium (1% yeast
554 peptone, 0.1% glucose, 1.4 M sorbitol, 50 mM potassium phosphate, pH 7.5, 50 mM 2-
555 mercaptoethanol) supplemented with yeast lytic enzyme (Zymo Research) at 1 mg/g of wet cell
556 pellet, to a final concentration of 8 mL/g of wet cells and incubated for ~40 min at 37°C with
557 gentle agitation. Spheroplasts were recovered by centrifugation and washed once in recovery
558 medium (1% yeast peptone, 0.1 % glucose, 1 M sorbitol). Permeabilization was achieved by
559 osmotic lysis in the presence of osmotic support. The spheroplast pellet was resuspended with
560 ice-cold spheroplast lysis buffer (100 mM potassium acetate, 200 mM sorbitol, 20 mM HEPES-
561 KOH, pH 7.2, 2 mM $MgCl_2$) at a concentration of 5 mL/75 OD_{600} unit cell equivalents. The slurry
562 was pipetted up and down with moderate force 5-10 times and incubated on ice for 20 min to
563 osmotic equilibration. Permeabilized yeast cells (PYCs) were collected by centrifugation at 3,000
564 × *g* for 5 min at 4°C, and the supernatant was thoroughly removed. PYCs were washed twice
565 with TBPS (115 mM potassium acetate, 2.5 mM magnesium acetate, 0.25 M sorbitol, 1×
566 cOmplete protease inhibitor cocktail (Roche), 25 mM HEPES, pH 7.2) and resuspended in TBPS
567 at a concentration of 25 µL/5 OD_{600} unit cell equivalents.
568 For yeast cytosols, spheroplasts were lysed with ice-cold 20 mM HEPES-KOH, pH 7.4, at
569 a concentration of 210 µL per 75 OD_{600} unit cell equivalents. The slurry was pipetted 30 times
570 with a 1 mL pipet to ensure efficient lysis. The resultant lysate was clarified by centrifugation at
571 3,000 × *g* for 5 min at 4°C, and the supernatant was collected and subjected to centrifugation at
572 100,000 × *g* for 1 h to produce a 100 k*g*S supernatant (S100) of yeast cytosol. Protein
573 concentration was determined by a bicinchoninic acid assay (Pierce) and normalized to 4

574 mg/mL with addition of 10× transport buffer (250 mM HEPES-KOH, pH 7.2, 1.15 M potassium
575 acetate, 25 mM $MgCl_2$, 2.5 M sorbitol) and cOmplete protease inhibitor cocktail to 1×
576 concentration.

577 Reaction conditions were as follows: 100 µL of PYCs, 100 µL of wild-type cytosol, 100 µL
578 of a 4× ATP regenerating system (4 mM ATP, 0.4 mM GTP, 80 mM creatine phosphate, 4 U
579 creatine phosphate kinase (Sigma)), and 100 µL of 2× TBPS were mixed on ice. The reaction was
580 initiated by incubation at room temperature for 90 min, and chilling the samples on ice
581 terminated the reaction. After the reaction was terminated, the PYCs were pelleted by
582 centrifugation at 13,000 × *g* for 5 min at 4°C. To recover PPVs, the supernatant was subjected to
583 centrifugation at 200,000 × *g* for 1 h at 4°C. The pellet was resuspended in 2× sample buffer (4%
584 SDS, 0.15 M Tris-HCl, pH 6.8, 4 mM EDTA, 20% glycerol, 2% 2-mercaptoethanol, 0.02%
585 bromophenol blue) before being resolved by SDS-PAGE.

586 To complement PPV budding defects, cytosols were mixed 1:1 at 4˚C directly before
587 addition to the reaction. For experiments with apyrase, PYCs and cytosols were incubated
588 separately with 1 U of apyrase (Sigma) and resuspended in reaction buffer (25 mM HEPES-KOH,
589 pH 7.2, 115 mM potassium acetate, 2.5 mM $MgCl_2$, 250 mM sorbitol) for 20 min before starting
590 the reaction. For experiments in which exogenous ATP was added back, only apyrase-treated
591 PYCs that had been washed once in reaction buffer were used. Alphaview (ProteinSimple) was
592 used to quantify the chemiluminescence signal with values normalized between the negative
593 *pex19*Δ PYCs only control (set to 0), and the positive *wild-type* cytosol plus ATP control (set to
594 100). Experiments were performed in triplicate.

595 **Online supplemental material**

596 Fig. S1 contains supporting data to show additional electron micrographs of the ESCRT-III
597 deletion mutants revealing peroxisome morphology defects. Fig. S2 contains supporting data to
598 show the budding efficiencies of PPVs from reactions containing cytosols isolated from ESCRT
599 deletion strains. Fig. S3 contains supporting data to show the levels of Pex19 in ESCRT deletion
600 mutants. Table S1 contains supplemental information summarizing the results of ESCRT
601 deletion mutants from previous genomic screens for peroxisome function. Table S2 contains
602 supplemental information on the normalized *Z*-scores for all strains measured by ODELAY!.
603 Table S3 contains supplemental information on the genetic background of the yeast strains
604 used in this study, as well as their origin of derivation.

605 **Acknowledgments**

606 We thank Alexis Kaushansky, Sanjeev Kumar, Maxwell Neal, and the Aitchison laboratory for
607 helpful discussion and feedback on the manuscript. We gratefully acknowledge the technical
608 assistance of Elena Savidov.

609 This work was supported by a Foundation Grant from the Canadian Institutes of Health
610 Research (CIHR) to R.A.R. and by grants P50 GM076547 and P41 GM109824 from the National
611 Institutes of Health to J.D.A. F.D.M is a postdoctoral fellow of the CIHR. The support of Ian
612 Tolmie and Jennifer Black is gratefully acknowledged, and this paper is dedicated to the
613 memory their son, Dane Tolmie.

614 The authors declare no competing financial interests.

615 Author contributions: F.D.M., R.A.R, and J.D.A. designed the experiments, analyzed the
616 results and wrote the manuscript. F.D.M. performed the experiments. R.A.R performed the EM
617 experiments. T.H. performed the ODELAY! experiments and analysis. K.M.S and L.R.M assisted

618 with the experiments. R.A.S contributed to the experimental design and analysis. All authors

619 read and commented on the manuscript.

620 **References**

621 Adolf, F., A. Herrmann, A. Hellwig, R. Beck, B. Brugger, and F.T. Wieland. 2013. Scission of COPI
622 and COPII vesicles is independent of GTP hydrolysis. *Traffic*. 14:922–932.
623 Agrawal, G., S.N. Fassas, Z.J. Xia, and S. Subramani. 2016. Distinct requirements for intra-ER
624 sorting and budding of peroxisomal membrane proteins from the ER. *J. Cell Biol*.
625 212:335–348.
626 Agrawal, G., S. Joshi, and S. Subramani. 2011. Cell-free sorting of peroxisomal membrane
627 proteins from the endoplasmic reticulum. *Proc. Natl. Acad. Sci. USA*. 108:9113–9118.
628 Agrawal, G., H.H. Shang, Z.J. Xia, and S. Subramani. 2017. Functional regions of the peroxin
629 Pex19 necessary for peroxisome biogenesis. *J. Biol. Chem*. 292:11547–11560.
630 Agrawal, G., and S. Subramani. 2016. *De novo* peroxisome biogenesis: Evolving concepts and
631 conundrums. *Biochim. Biophys. Acta*. 1863:892–901.
632 Aitchison, J.D., G. Blobel, and M.P. Rout. 1995. Nup120p: a yeast nucleoporin required for NPC
633 distribution and mRNA transport. *J. Cell Biol*. 131:1659–1675.
634 Babst, M., D.J. Katzmann, E.J. Estepa-Sabal, T. Meerloo, and S.D. Emr. 2002a. ESCRT-III: an
635 endosome-associated heterooligomeric protein complex required for MVB sorting. *Dev.*
636 *Cell*. 3:271–282.
637 Babst, M., D.J. Katzmann, W.B. Snyder, B. Wendland, and S.D. Emr. 2002b. Endosome-
638 associated complex, ESCRT-II, recruits transport machinery for protein sorting at the
639 multivesicular body. *Dev. Cell*. 3:283–289.
640 Babst, M., T.K. Sato, L.M. Banta, and S.D. Emr. 1997. Endosomal transport function in yeast
641 requires a novel AAA-type ATPase, Vps4p. *EMBO J*. 16:1820–1831.
642 Bauer, S.T., K.E. McQueeney, T. Patel, and M.T. Morris. 2017. Localization of a trypanosome
643 peroxin to the endoplasmic reticulum. *J. Eukaryot. Microbiol*. 64:97–105.
644 Bolte, S., and F.P. Cordelieres. 2006. A guided tour into subcellular colocalization analysis in
645 light microscopy. *J. Microsc*. 224:213–232.
646 Briza, P., E. Bogengruber, A. Thur, M. Rutzler, M. Munsterkotter, I.W. Dawes, and M.
647 Breitenbach. 2002. Systematic analysis of sporulation phenotypes in 624 non-lethal
648 homozygous deletion strains of *Saccharomyces cerevisiae*. *Yeast*. 19:403–422.
649 Carlton, J.G., and J. Martin-Serrano. 2007. Parallels between cytokinesis and retroviral budding:
650 a role for the ESCRT machinery. *Science*. 316:1908–1912.
651 Colasante, C., J. Chen, B. Ahlemeyer, and E. Baumgart-Vogt. 2015. Peroxisomes in
652 cardiomyocytes and the peroxisome / peroxisome proliferator-activated receptor-loop.
653 *Thromb. Haemost*. 113:452–463.
654 Costanzo, M., B. VanderSluis, E.N. Koch, A. Baryshnikova, C. Pons, G. Tan, W. Wang, M. Usaj, J.
655 Hanchard, S.D. Lee, et al. 2016. A global genetic interaction network maps a wiring
656 diagram of cellular function. *Science*. 353.

657 Curwin, A.J., N. Brouwers, Y.A.M. Alonso, D. Teis, G. Turacchio, S. Parashuraman, P. Ronchi, and
658 V. Malhotra. 2016. ESCRT-III drives the final stages of CUPS maturation for
659 unconventional protein secretion. *eLife*. 5.
660 David, C., J. Koch, S. Oeljeklaus, A. Laernsack, S. Melchior, S. Wiese, A. Schummer, R. Erdmann,
661 B. Warscheid, and C. Brocard. 2013. A combined approach of quantitative interaction
662 proteomics and live-cell imaging reveals a regulatory role for endoplasmic reticulum (ER)
663 reticulon homology proteins in peroxisome biogenesis. *Mol. Cell. Proteomics*.
664 12:2408–2425.
665 De Craemer, D., M. Pauwels, and F. Roels. 1993. Peroxisomes in cirrhosis of the human liver: a
666 cytochemical, ultrastructural and quantitative study. *Hepatology*. 17:404–410.
667 Delmaghani, S., J. Defourny, A. Aghaie, M. Beurg, D. Dulon, N. Thelen, I. Perfettini, T. Zelles, M.
668 Aller, A. Meyer, et al. 2015. Hypervulnerability to sound exposure through impaired
669 adaptive proliferation of peroxisomes. *Cell*. 163:894–906.
670 Di Cara, F., A. Sheshachalam, N.E. Braverman, R.A. Rachubinski, and A.J. Simmonds. 2017.
671 Peroxisome-mediated metabolism is required for immune response to microbial
672 infection. *Immunity*. 47:93–106.
673 Dilworth, D.J., A. Suprapto, J.C. Padovan, B.T. Chait, R.W. Wozniak, M.P. Rout, and J.D.
674 Aitchison. 2001. Nup2p dynamically associates with the distal regions of the yeast
675 nuclear pore complex. *J. Cell Biol*. 153:1465–1478.
676 Distel, B., R. Erdmann, S.J. Gould, G. Blobel, D.I. Crane, J.M. Cregg, G. Dodt, Y. Fujiki, J.M.
677 Goodman, W.W. Just, et al. 1996. A unified nomenclature for peroxisome biogenesis
678 factors. *J. Cell Biol*. 135:1–3.
679 Dixit, E., S. Boulant, Y. Zhang, A.S. Lee, C. Odendall, B. Shum, N. Hacohen, Z.J. Chen, S.P.
680 Whelan, M. Fransen, et al.. 2010. Peroxisomes are signaling platforms for antiviral
681 innate immunity. *Cell*. 141:668–681.
682 Dixon, S.J., M. Costanzo, A. Baryshnikova, B. Andrews, and C. Boone. 2009. Systematic mapping
683 of genetic interaction networks. *Ann. Rev. Genet*. 43:601–625.
684 Drees, B.L., V. Thorsson, G.W. Carter, A.W. Rives, M.Z. Raymond, I. Avila-Campillo, P. Shannon,
685 and T. Galitski. 2005. Derivation of genetic interaction networks from quantitative
686 phenotype data. *Genome Biol*. 6:R38.
687 Duden, R., L. Kajikawa, L. Wuestehube, and R. Schekman. 1998. ε-COP is a structural
688 component of coatomer that functions to stabilize α-COP. *EMBO J*. 17:985–995.
689 Edelstein, A.D., M.A. Tsuchida, N. Amodaj, H. Pinkard, R.D. Vale, and N. Stuurman. 2014.
690 Advanced methods of microscope control using μManager software. *J. Biol. Methods*.
691 1:e10.
692 Fagarasanu, A., M. Fagarasanu, G.A. Eitzen, J.D. Aitchison, and R.A. Rachubinski. 2006. The
693 peroxisomal membrane protein Inp2p is the peroxisome-specific receptor for the
694 myosin V motor Myo2p of *Saccharomyces cerevisiae*. *Dev. Cell*. 10:587–600.
695 Fagarasanu, A., F.D. Mast, B. Knoblach, Y. Jin, M.J. Brunner, M.R. Logan, J.N. Glover, G.A. Eitzen,
696 J.D. Aitchison, L.S. Weisman, et al. 2009. Myosin-driven peroxisome partitioning in *S.*
697 *cerevisiae*. *J. Cell Biol*. 186:541–554.
698 Fakieh, M.H., P.J. Drake, J. Lacey, J.M. Munck, A.M. Motley, and E.H. Hettema. 2013. Intra-ER
699 sorting of the peroxisomal membrane protein Pex3 relies on its luminal domain. *Biol.*
700 *Open*. 2:829–837.

701 Farré, J.C., K. Carolino, O.V. Stasyk, O.G. Stasyk, Z. Hodzic, G. Agrawal, A. Till, M. Proietto, J.
702 Cregg, A.A. Sibirny, et al. 2017. A new yeast peroxin, Pex36, a functional homolog of
703 mammalian PEX16, functions in the ER-to-peroxisome traffic of peroxisomal membrane
704 proteins. *J. Mol. Biol*. 429:3743–3762.
705 Gari, E., L. Piedrafita, M. Aldea, and E. Herrero. 1997. A set of vectors with a tetracycline-
706 regulatable promoter system for modulated gene expression in *Saccharomyces*
707 *cerevisiae*. *Yeast*. 13:837–848.
708 Garrus, J.E., U.K. von Schwedler, O.W. Pornillos, S.G. Morham, K.H. Zavitz, H.E. Wang, D.A.
709 Wettstein, K.M. Stray, M. Cote, R.L. Rich, et al. 2001. Tsg101 and the vacuolar protein
710 sorting pathway are essential for HIV-1 budding. *Cell*. 107:55–65.
711 Giaever, G., A.M. Chu, L. Ni, C. Connelly, L. Riles, S. Véronneau, S. Dow, A. Lucau-Danila, K.
712 Anderson, B. André, et al. 2002. Functional profiling of the *Saccharomyces cerevisiae*
713 genome. *Nature*. 418:387–391.
714 Guizetti, J., L. Schermelleh, J. Mantler, S. Maar, I. Poser, H. Leonhardt, T. Muller-Reichert, and
715 D.W. Gerlich. 2011. Cortical constriction during abscission involves helices of ESCRT-III-
716 dependent filaments. *Science*. 331:1616–1620.
717 Guther, M.L., M.D. Urbaniak, A. Tavendale, A. Prescott, and M.A. Ferguson. 2014. High-
718 confidence glycosome proteome for procyclic form *Trypanosoma brucei* by epitope-tag
719 organelle enrichment and SILAC proteomics. *J. Proteome Res*. 13:2796–2806.
720 Halbach, A., C. Landgraf, S. Lorenzen, K. Rosenkranz, R. Volkmer-Engert, R. Erdmann, and H.
721 Rottensteiner. 2006. Targeting of the tail-anchored peroxisomal membrane proteins
722 PEX26 and PEX15 occurs through C-terminal PEX19-binding sites. *J. Cell Sci*.
723 119:2508–2517.
724 Henne, W.M., N.J. Buchkovich, and S.D. Emr. 2011. The ESCRT pathway. *Dev. Cell*. 21:77–91.
725 Herricks, T., D.J. Dilworth, F.D. Mast, S. Li, J.J. Smith, A.V. Ratushny, and J.D. Aitchison. 2017a.
726 One-cell doubling evaluation by living arrays of yeast, ODELAY! *G3 (Bethesda)*.
727 7:279–288.
728 Herricks, T., F.D. Mast, S. Li, and J.D. Aitchison. 2017b. ODELAY: A large-scale method for multi-
729 parameter quantification of yeast growth. *J. Vis. Exp*., e55879.
730 Hettema, E.H., W. Girzalsky, M. van Den Berg, R. Erdmann, and B. Distel. 2000. *Saccharomyces*
731 *cerevisiae* Pex3p and Pex19p are required for proper localization and stability of
732 peroxisomal membrane proteins. *EMBO J*. 19:223–233.
733 Hoepfner, D., D. Schildknegt, I. Braakman, P. Philippsen, and H.F. Tabak. 2005. Contribution of
734 the endoplasmic reticulum to peroxisome formation. *Cell*. 122:85–95.
735 Hu, J., A. Baker, B. Bartel, N. Linka, R.T. Mullen, S. Reumann, and B.K. Zolman. 2012. Plant
736 peroxisomes: biogenesis and function. *Plant Cell*. 24:2279–2303.
737 Igual, J.C., E. Matallana, C. Gonzalez-Bosch, L. Franco, and J.E. Perez-Ortin. 1991. A new glucose-
738 repressible gene identified from the analysis of chromatin structure in deletion mutants
739 of yeast *SUC2* locus. *Yeast*. 7:379–389.
740 Jan, C.H., C.C. Williams, and J.S. Weissman. 2014. Principles of ER cotranslational translocation
741 revealed by proximity-specific ribosome profiling. *Science*. 346:1257521.
742 Janke, C., M.M. Magiera, N. Rathfelder, C. Taxis, S. Reber, H. Maekawa, A. Moreno-Borchart, G.
743 Doenges, E. Schwob, E. Schiebel, et al. 2004. A versatile toolbox for PCR-based tagging

744 of yeast genes: new fluorescent proteins, more markers and promoter substitution
745 cassettes. *Yeast*. 21:947–962.
746 Jimenez, A.J., P. Maiuri, J. Lafaurie-Janvore, S. Divoux, M. Piel, and F. Perez. 2014. ESCRT
747 machinery is required for plasma membrane repair. *Science*. 343:1247136.
748 Joshi, A.S., X. Huang, V. Choudhary, T.P. Levine, J. Hu, and W.A. Prinz. 2016. A family of
749 membrane-shaping proteins at ER subdomains regulates pre-peroxisomal vesicle
750 biogenesis. *J. Cell Biol*. 215:515–529.
751 Jung, S., M. Marelli, R.A. Rachubinski, D.R. Goodlett, and J.D. Aitchison. 2010. Dynamic changes
752 in the subcellular distribution of Gpd1p in response to cell stress. *J. Biol. Chem*.
753 285:6739–6749.
754 Kaewsapsak, P., D.M. Shechner, W. Mallard, J.L. Rinn, and A.Y. Ting. 2017. Live-cell mapping of
755 organelle-associated RNAs via proximity biotinylation combined with protein-RNA
756 crosslinking. *eLife*. 6:e29224.
757 Katzmann, D.J., M. Babst, and S.D. Emr. 2001. Ubiquitin-dependent sorting into the
758 multivesicular body pathway requires the function of a conserved endosomal protein
759 sorting complex, ESCRT-I. *Cell*. 106:145–155.
760 Katzmann, D.J., C.J. Stefan, M. Babst, and S.D. Emr. 2003. Vps27 recruits ESCRT machinery to
761 endosomes during MVB sorting. *J. Cell Biol*. 162:413–423.
762 Kao, Y.T., K.L. Gonzalez, and B. Bartel. 2018. Peroxisome function, biogenesis, and dynamics in
763 plants. *Plant Physiol*. 176:162–177.
764 Kim, P.K., R.T. Mullen, U. Schumann, and J. Lippincott-Schwartz. 2006. The origin and
765 maintenance of mammalian peroxisomes involves a de novo PEX16-dependent pathway
766 from the ER. *J. Cell Biol*. 173:521–532.
767 Kumar, S., R. de Boer, and I. van der Klei. 2018. Yeast cells contain a heterogeneous population
768 of peroxisomes that segregate asymmetrically during cell division. *J. Cell Sci*. In press.
769 Lam, S.K., N. Yoda, and R. Schekman. 2010. A vesicle carrier that mediates peroxisome protein
770 traffic from the endoplasmic reticulum. *Proc. Natl. Acad. Sci. USA*. 107:21523–21528.
771 Lee, J.A., A. Beigneux, S.T. Ahmad, S.G. Young, and F.B. Gao. 2007. ESCRT-III dysfunction causes
772 autophagosome accumulation and neurodegeneration. *Curr. Biol*. 17:1561–1567.
773 Li, X., E. Baumgart, J.C. Morrell, G. Jimenez-Sanchez, D. Valle, and S.J. Gould. 2002. PEX11β
774 deficiency is lethal and impairs neuronal migration but does not abrogate peroxisome
775 function. *Mol. Cell. Biol*. 22:4358–4365.
776 Loncle, N., M. Agromayor, J. Martin-Serrano, and D.W. Williams. 2015. An ESCRT module is
777 required for neuron pruning. *Sci. Rep*. 5:8461.
778 Mani, R., R.P. St. Onge, J.L. Hartman IV, G. Giaever, and F.P. Roth. 2008. Defining genetic
779 interaction. *Proc. Natl. Acad. Sci. USA*. 105:3461–3466.
780 Manjithaya, R., C. Anjard, W.F. Loomis, and S. Subramani. 2010. Unconventional secretion of
781 *Pichia pastoris* Acb1 is dependent on GRASP protein, peroxisomal functions, and
782 autophagosome formation. *J. Cell Biol*. 188:537–546.
783 Mast, F.D., A. Fagarasanu, B. Knoblach, and R.A. Rachubinski. 2010. Peroxisome biogenesis:
784 something old, something new, something borrowed. *Physiology*. 25:347–356.
785 Mast, F.D., A. Jamakhandi, R.A. Saleem, D.J. Dilworth, R.S. Rogers, R.A. Rachubinski, and J.D.
786 Aitchison. 2016. Peroxins Pex30 and Pex29 dynamically associate with reticulons to

787 regulate peroxisome biogenesis from the endoplasmic reticulum. *J. Biol. Chem*.
788 291:15408–15427.
789 Mast, F.D., R.A. Rachubinski, and J.D. Aitchison. 2015. Signaling dynamics and peroxisomes.
790 *Curr. Opin. Cell Biol*. 35:131–136.
791 Mayerhofer, P.U., M. Bano-Polo, I. Mingarro, and A.E. Johnson. 2016. Human peroxin PEX3 is
792 co-translationally Integrated into the ER and exits the ER in budding vesicles. *Traffic*.
793 17:117–130.
794 McCullough, J., A.K. Clippinger, N. Talledge, M.L. Skowyra, M.G. Saunders, T.V. Naismith, L.A.
795 Colf, P. Afonine, C. Arthur, W.I. Sundquist, et al. 2015. Structure and membrane
796 remodeling activity of ESCRT-III helical polymers. *Science*. 350:1548–1551.
797 Meinecke, M., C. Cizmowski, W. Schliebs, V. Kruger, S. Beck, R. Wagner, and R. Erdmann. 2010.
798 The peroxisomal importomer constitutes a large and highly dynamic pore. *Nat. Cell Biol*.
799 12:273–277.
800 Mnaimneh, S., A.P. Davierwala, J. Haynes, J. Moffat, W.T. Peng, W. Zhang, X. Yang, J. Pootoolal,
801 G. Chua, A. Lopez, et al. 2004. Exploration of essential gene functions via titratable
802 promoter alleles. *Cell*. 118:31–44.
803 Motley, A.M., P.C. Galvin, L. Ekal, J.M. Nuttall, and E.H. Hettema. 2015. Reevaluation of the role
804 of Pex1 and dynamin-related proteins in peroxisome membrane biogenesis. *J. Cell Biol*.
805 211:1041–1056.
806 Motley, A.M., and E.H. Hettema. 2007. Yeast peroxisomes multiply by growth and division. *J.*
807 *Cell Biol*. 178:399–410.
808 Motley, A.M., G.P. Ward, and E.H. Hettema. 2008. Dnm1p-dependent peroxisome fission
809 requires Caf4p, Mdv1p and Fis1p. *J. Cell Sci*. 121:1633–1640.
810 Nichols, B.J., C. Ungermann, H.R. Pelham, W.T. Wickner, and A. Haas. 1997. Homotypic vacuolar
811 fusion mediated by t- and v-SNAREs. *Nature*. 387:199–202.
812 Nixon-Abell, J., C.J. Obara, A.V. Weigel, D. Li, W.R. Legant, C.S. Xu, H.A. Pasolli, K. Harvey, H.F.
813 Hess, E. Betzig, et al. 2016. Increased spatiotemporal resolution reveals highly dynamic
814 dense tubular matrices in the peripheral ER. *Science*. 354:aaf3928.
815 Odendall, C., E. Dixit, F. Stavru, H. Bierne, K.M. Franz, A.F. Durbin, S. Boulant, L. Gehrke, P.
816 Cossart, and J.C. Kagan. 2014. Diverse intracellular pathogens activate type III interferon
817 expression from peroxisomes. *Nat. Immunol*. 15:717–726.
818 Olmos, Y., L. Hodgson, J. Mantell, P. Verkade, and J.G. Carlton. 2015. ESCRT-III controls nuclear
819 envelope reformation. *Nature*. 522:236–239.
820 Perry, R.J., F.D. Mast, and R.A. Rachubinski. 2009. Endoplasmic reticulum-associated secretory
821 proteins Sec20p, Sec39p, and Dsl1p are involved in peroxisome biogenesis. *Euk. Cell*.
822 8:830–843.
823 Reumann, S., and B. Bartel. 2016. Plant peroxisomes: recent discoveries in functional
824 complexity, organelle homeostasis, and morphological dynamics. *Curr. Opin. Plant Biol*.
825 34:17–26.
826 Reumann, S., and A.P. Weber. 2006. Plant peroxisomes respire in the light: some gaps of the
827 photorespiratory C2 cycle have become filled – others remain. *Biochem. Biophys. Acta*.
828 1763:1496–1510.
829 Rothstein, R.J., R.E. Esposito, and M.S. Esposito. 1977. The effect of ochre suppression on
830 meiosis and ascospore formation in *Saccharomyces*. *Genetics*. 85:35–54.

831 Rusten, T.E., T. Vaccari, K. Lindmo, L.M. Rodahl, I.P. Nezis, C. Sem-Jacobsen, F. Wendler, J.P.
832 Vincent, A. Brech, D. Bilder, et al. 2007. ESCRTs and Fab1 regulate distinct steps of
833 autophagy. *Curr. Biol*. 17:1817–1825.
834 Saleem, R.A., B. Knoblach, F.D. Mast, J.J. Smith, J. Boyle, C.M. Dobson, R. Long-O'Donnell, R.A.
835 Rachubinski, and J.D. Aitchison. 2008. Genome-wide analysis of signaling networks
836 regulating fatty acid-induced gene expression and organelle biogenesis. *J. Cell Biol*.
837 181:281–292.
838 Saleem, R.A., R. Long-O'Donnell, D.J. Dilworth, A.M. Armstrong, A.P. Jamakhandi, Y. Wan, T.A.
839 Knijnenburg, A. Niemisto, J. Boyle, R.A. Rachubinski, et al. 2010. Genome-wide analysis
840 of effectors of peroxisome biogenesis. *PLOS ONE*. 5:e11953.
841 Sato, K., and A. Nakano. 2002. Emp47p and its close homolog Emp46p have a tyrosine-
842 containing endoplasmic reticulum exit signal and function in glycoprotein secretion in
843 *Saccharomyces cerevisiae*. *Mol. Biol. Cell*. 13:2518–2532.
844 Scheffer, L.L., S.C. Sreetama, N. Sharma, S. Medikayala, K.J. Brown, A. Defour, and J.K. Jaiswal.
845 2014. Mechanism of Ca^{2+}-triggered ESCRT assembly and regulation of cell membrane
846 repair. *Nat. Commun*. 5:5646.
847 Schoneberg, J., I.H. Lee, J.H. Iwasa, and J.H. Hurley. 2016. Reverse-topology membrane scission
848 by the ESCRT proteins. *Nat. Rev. Mol. Cell Biol*. 18:5–17.
849 Schrader, M., J.L. Costello, L.F. Godinho, A.S. Azadi, and M. Islinger. 2016. Proliferation and
850 fission of peroxisomes - An update. *Biochim. Biophys. Acta*. 1863:971–983.
851 Schrul, B., and R.R. Kopito. 2016. Peroxin-dependent targeting of a lipid-droplet-destined
852 membrane protein to ER subdomains. *Nat. Cell Biol*. 18:740–751.
853 Schuldiner, M., and M. Bohnert. 2017. A different kind of love - lipid droplet contact sites.
854 *Biochim. Biophys. Acta*. 1862:1188–1196.
855 Schuldiner, M., S.R. Collins, N.J. Thompson, V. Denic, A. Bhamidipati, T. Punna, J. Ihmels, B.
856 Andrews, C. Boone, J.F. Greenblatt, et al. 2005. Exploration of the function and
857 organization of the yeast early secretory pathway through an epistatic miniarray profile.
858 *Cell*. 123:507–519.
859 Schuldiner, M., J. Metz, V. Schmid, V. Denic, M. Rakwalska, H.D. Schmitt, B. Schwappach, and
860 J.S. Weissman. 2008. The GET complex mediates insertion of tail-anchored proteins into
861 the ER membrane. *Cell*. 134:634–645.
862 Shaner, N.C., R.E. Campbell, P.A. Steinbach, B.N. Giepmans, A.E. Palmer, and R.Y. Tsien. 2004.
863 Improved monomeric red, orange and yellow fluorescent proteins derived from
864 *Discosoma* sp. red fluorescent protein. *Nat. Biotechnol*. 22:1567–1572.
865 Smith, J.J., and J.D. Aitchison. 2013. Peroxisomes take shape. *Nat. Rev. Mol. Cell Biol*.
866 14:803–817.
867 Smith, J.J., M. Marelli, R.H. Christmas, F.J. Vizeacoumar, D.J. Dilworth, T. Ideker, T. Galitski, K.
868 Dimitrov, R.A. Rachubinski, and J.D. Aitchison. 2002. Transcriptome profiling to identify
869 genes involved in peroxisome assembly and function. *J. Cell Biol*. 158:259–271.
870 Smith, J.J., Y. Sydorskyy, M. Marelli, D. Hwang, H. Bolouri, R.A. Rachubinski, and J.D. Aitchison.
871 2006. Expression and functional profiling reveal distinct gene classes involved in fatty
872 acid metabolism. *Mol. Syst. Biol*. 2:2006 0009.
873 South, S.T., K.A. Sacksteder, X. Li, Y. Liu, and S.J. Gould. 2000. Inhibitors of COPI and COPII do
874 not block PEX3-mediated peroxisome synthesis. *J. Cell Biol*. 149:1345–1360.

875 Spang, A. 2008. The life cycle of a transport vesicle. *Cell Mol. Life Sci*. 65:2781–2789.
876 Tam, Y.Y.C., A. Fagarasanu, M. Fagarasanu, and R.A. Rachubinski. 2005. Pex3p initiates the
877 formation of a preperoxisomal compartment from a subdomain of the endoplasmic
878 reticulum in *Saccharomyces cerevisiae*. *J. Biol. Chem*. 280:34933–34939.
879 Tam, Y.Y.C, J.C. Torres-Guzman, F.J. Vizeacoumar, J.J. Smith, M. Marelli, J.D. Aitchison, and R.A.
880 Rachubinski. 2003. Pex11-related proteins in peroxisome dynamics: a role for the novel
881 peroxin Pex27p in controlling peroxisome size and number in *Saccharomyces cerevisiae*.
882 *Mol. Biol. Cell*. 14:4089–4102.
883 Tang, S., W.M. Henne, P.P. Borbat, N.J. Buchkovich, J.H. Freed, Y. Mao, J.C. Fromme, and S.D.
884 Emr. 2015. Structural basis for activation, assembly and membrane binding of ESCRT-III
885 Snf7 filaments. *eLife*. 4:e12548.
886 Thoms, S., I. Harms, K.U. Kalies, and J. Gartner. 2012. Peroxisome formation requires the
887 endoplasmic reticulum channel protein Sec61. *Traffic*. 13:599–609.
888 Titorenko, V.I., H. Chan, and R.A. Rachubinski. 2000. Fusion of small peroxisomal vesicles in
889 vitro reconstructs an early step in the in vivo multistep peroxisome assembly pathway of
890 *Yarrowia lipolytica*. *J. Cell Biol*. 148:29–44.
891 Titorenko, V.I., and R.A. Rachubinski. 1998. Mutants of the yeast *Yarrowia lipolytica* defective in
892 protein exit from the endoplasmic reticulum are also defective in peroxisome
893 biogenesis. *Mol. Cell. Biol*. 18:2789–2803.
894 Titorenko, V.I., and R.A. Rachubinski. 2000. Peroxisomal membrane fusion requires two AAA
895 family ATPases, Pex1p and Pex6p. *J. Cell Biol*. 150:881–886.
896 Tripathi, D.N., and C.L. Walker. 2016. The peroxisome as a cell signaling organelle. *Curr. Opin.*
897 *Cell Biol*. 39:109–112.
898 van der Zand, A., I. Braakman, and H.F. Tabak. 2010. Peroxisomal membrane proteins insert
899 into the endoplasmic reticulum. *Mol. Biol. Cell*. 21:2057–2065.
900 van der Zand, A., J. Gent, I. Braakman, and H.F. Tabak. 2012. Biochemically distinct vesicles from
901 the endoplasmic reticulum fuse to form peroxisomes. *Cell*. 149:397–409.
902 Vietri, M., K.O. Schink, C. Campsteijn, C.S. Wegner, S.W. Schultz, L. Christ, S.B. Thoresen, A.
903 Brech, C. Raiborg, and H. Stenmark. 2015. Spastin and ESCRT-III coordinate mitotic
904 spindle disassembly and nuclear envelope sealing. *Nature*. 522:231–235.
905 Webster, B.M., P. Colombi, J. Jager, and C.P. Lusk. 2014. Surveillance of nuclear pore complex
906 assembly by ESCRT-III/Vps4. *Cell*. 159:388–401.
907 Weibel, E.R., and R.P. Bolender. 1973. Stereological techniques for electron microscopic
908 morphometry. *In* Principles and Techniques of Electron Microscopy. M.A. Hayat, editor.
909 Van Nostrand Reinhold, New York, NY. 237–296.
910 Weller, S., S.J. Gould, and D. Valle. 2003. Peroxisome biogenesis disorders. *Ann. Rev. Genomics*
911 *Hum. Genet*. 4:165–211.
912 Wollert, T., C. Wunder, J. Lippincott-Schwartz, and J.H. Hurley. 2009. Membrane scission by the
913 ESCRT-III complex. *Nature*. 458:172–177.
914 Young, J.M., J.W. Nelson, J. Cheng, W. Zhang, S. Mader, C.M. Davis, R.S. Morrison, and N.J.
915 Alkayed. 2015. Peroxisomal biogenesis in ischemic brain. *Antioxid. Redox Signal*.
916 22:109–120.
917 Zhang, J., J. Kim, A. Alexander, S. Cai, D.N. Tripathi, R. Dere, A.R. Tee, J. Tait-Mulder, A. Di
918 Nardo, J.M. Han, et al. 2013. A tuberous sclerosis complex signalling node at the

919 peroxisome regulates mTORC1 and autophagy in response to ROS. *Nat. Cell Biol*.
920 15:1186–1196.
921 Zhang, J., D.N. Tripathi, J. Jing, A. Alexander, J. Kim, R.T. Powell, R. Dere, J. Tait-Mulder, J.H. Lee,
922 T.T. Paull, et al. 2015. ATM functions at the peroxisome to induce pexophagy in
923 response to ROS. *Nat. Cell Biol*. 17:1259-1269.

924 ## Figure legends

925 **Figure 1. ESCRT-III mutants exhibit oleate-specific growth defects.** Doubling times of individual
926 yeast cells growing into colonies on solid-phase medium containing either glucose or oleic acid
927 as sole carbon source were measured with ODELAY!. A population-derived *Z*-score and SEM for
928 each strain are plotted with measurements from glucose-containing medium on the *x*-axis
929 against measurements from oleic acid-containing medium on the *y*-axis from 8 biological
930 replicates per growth condition. (A) ODELAY! results for deletion strains derived from the
931 *BY4742* parental strain. (B) ODELAY! results for select ESCRT deletion strains derived from the
932 *W303* parental strain.

933 **Figure 2. ESCRT-III deletion strains have populations of smaller and aberrant peroxisomes.** (A)
934 *Wild-type*, (B) *vps20*Δ and (C) *snf7*Δ cells were grown in medium containing oleic acid for 8 h to
935 induce the production of peroxisomes and prepared for EM. Representative cell ultrastructures
936 and organelle profiles are presented. Arrowheads in (B) and (C) point to aberrant vesicular
937 structures observed in *vps20*Δ and *snf7*Δ cells. Bar, 1 µm. (D–I) Morphometric analysis of
938 peroxisomes. For each strain analyzed, the areas of individual peroxisomes were determined
939 and used to calculate the numerical density of peroxisomes, which is the number of
940 peroxisomes per μm^3 of cell volume (Weibel and Bolender, 1973). Bar graphs display the

941 numerical density of peroxisomes (D) and the population distribution of the areas of
942 peroxisomes (E–I) for *wild-type* and ESCRT-III deletion strains.

943 **Figure 3. ESCRT-III positively regulates de novo peroxisome biogenesis.** (A) Genomically
944 encoded *PEX19* was placed under the control of a tetracycline-repressible tet_{07} promoter to
945 allow regulatable de novo peroxisome production in *wild-type*, *vps20*Δ, *snf7*Δ, *did4*Δ, *vps24*Δ,
946 and *ist1*Δ cells expressing Gpd1-GFP as a peroxisomal marker. Cells were imaged before
947 (steady-state) and after 24 h incubation with 4 µM DOX. Additional observations were made 4,
948 8, 12, and 24 h after removal of DOX. Scale bar, 5 µm. (B) The population distributions of
949 peroxisome densities per cell are depicted at each time point as interquartile box-and-whisker
950 blots. (C) The mean peroxisome density per strain over a time course of de novo peroxisome
951 biogenesis was plotted with error bars representing the SEM of 3 biological replicates.

952 **Figure 4. Pex19 dynamics are altered in ESCRT-III deletion mutants during de novo**
953 **peroxisome biogenesis.** Genomically encoded *PEX19* was placed under the control of a
954 tetracycline-repressible tet_{07} promoter to allow regulatable de novo peroxisome production in
955 *wild-type*, *vps20*Δ, *snf7*Δ, *did4*Δ, *vps24*Δ and *ist1*Δ cells. Whole cell lysates were prepared from
956 each strain before (steady-state) and after a 24 h incubation with 4 µM DOX. Additional whole
957 cell lysates were prepared 4, 8, 12 and 24 h after removal of DOX. Equal amounts of protein
958 from these whole cell lysates were resolved by SDS-PAGE, transferred to PVDF, and
959 immunoblotted for Pex19 and Kar2, which was used as a control for protein loading.

960 **Figure 5. ESCRT-III functions conditionally with *PEX19*.** Doubling times of individual yeast cells
961 growing into colonies on solid-phase YEPD medium with and without 4 µM DOX were measured

962 with ODELAY!. Strains grown in the presence of DOX were precultured for 24 h in the presence
963 of 4 µM DOX to turn off *PEX19* and deplete Pex19 levels from cells. A population-derived *Z*-
964 score and SEM for each strain are plotted on a phenotypic axis and summarized as a phenotypic
965 inequality defining the genetic interaction between the indicated genes from 4 biological
966 replicates per strain per growth condition.

967 **Figure 6. ESCRT-III components localize to sites of de novo peroxisome biogenesis.** (A) Snf7
968 localizes to sites of de novo peroxisome biogenesis. *Wild-type* cells expressing endogenously
969 tagged Pex3-GFP and Snf7-mCherry with tetracycline-repressible *PEX19* were imaged before
970 (control) and 1 h following an 18 h incubation with 2 µM DOX (recovery). Arrowheads point to
971 areas of colocalization between Pex3-GFP and Snf7-mCherry (see zoom window for
972 enlargement). For the merged image, calcofluor white staining (cyan) was used to demarcate
973 cell boundaries. Bar graphs report the percent overlap of Pex3-GFP puncta colocalizing with
974 Snf7-mCherry puncta with error bars representing the SEM of 3 biological replicates. Scale bar,
975 5 µm. (B) Same as (A), but with Did4-mCherry instead of Snf7-mCherry.

976 **Figure 7. ESCRT-III is required for PPV budding from the ER.** (A) Permeabilized *pex19*Δ yeast
977 cells (PYCs) containing microsomes and expressing Pex3-pA were incubated with the S100
978 fraction of cytosol isolated from *wild-type* (lanes 2-4), *vps25*Δ (lane 5), *vps20*Δ (lane 6), *snf7*Δ
979 (lane 7), *did4*Δ (lane 8), *vps24*Δ (lane 9) or *ist1*Δ (lane 10) for 90 min at room temperature in the
980 presence of an ATP-regenerating system. Controls included incubating the PYCs alone (lane 1),
981 with cytosol but no ATP (lane 2), or with cytosol and ATP but at 4˚C (lane 3). (B) As in (A), but
982 with the S100 fraction of cytosol isolated from *W303 wild-type* and deletion strains. (C and D)

983 Deficiencies in PPV budding are complemented by mixing the S100 fractions of defective
984 cytosols. PYCs were incubated with *wild-type* (lanes 2-4), *vps20Δ* (lanes 5, 8, and 9), *snf7*Δ
985 (lanes 6, 8, and 10), and *pex19*Δ (lanes 7, 9, and 10) S100 fractions of cytosol for 90 min at room
986 temperature in the presence of an ATP-regenerating system. Controls included incubating the
987 PYCs alone (lane 1), with cytosol but no ATP (lane 2), or with cytosol and ATP but at 4˚C (lane 3).
988 (E and F) *VPS20* and *SNF7* complement deficiencies in PPV budding in their respective deletion
989 mutants. PYCs were incubated with S100 fractions of cytosol from *wild-type* carrying pCM189
990 (lane 2), *vps20*Δ carrying pCM189 (lane 3) or pCM189-*VPS20* (lane 4), or *snf7*Δ carrying pCM189
991 (lane 5) or pCM189-*SNF7* (lane 6). (G) ATP is not required for PPV release but rather to recycle
992 scission components. PYCs expressing Pex3-GFP and the S100 fraction of cytosol isolated from
993 *wild-type* were pretreated with apyrase before starting the reaction (lanes 3 and 5). The
994 reaction was also sampled at the indicated times (lanes 6-10). For each panel, bar graphs
995 represent the relative % of PPV release in arbitrary units with error bars representing the SEM
996 of 3 biological replicates.

997 **Table 1. Average area and numerical density of peroxisomes or vesicular structures in cells of**
998 ***wild-type* and ESCRT-III deletion strains**

strain	cell area assayed (μm^2)	peroxisome count	numerical density of peroxisomes[#]	average area of peroxisomes (μm^2)
BY4742	1396.09	421	1.14	0.037
*vps20*Δ	1125.46	69[*]	0.39[*]	0.005[*]
*snf7*Δ	1144.83	89[*]	0.34[*]	0.018[*]

*did4*Δ	820.13	35	0.28	0.040
*vps24*Δ	933.70	138	0.51	0.044

999 * denotes vesicular structures, as no peroxisomes were observed in these strains.
1000 # number of peroxisomes per μm^3 of cell volume (Weibel and Bolender, 1973).

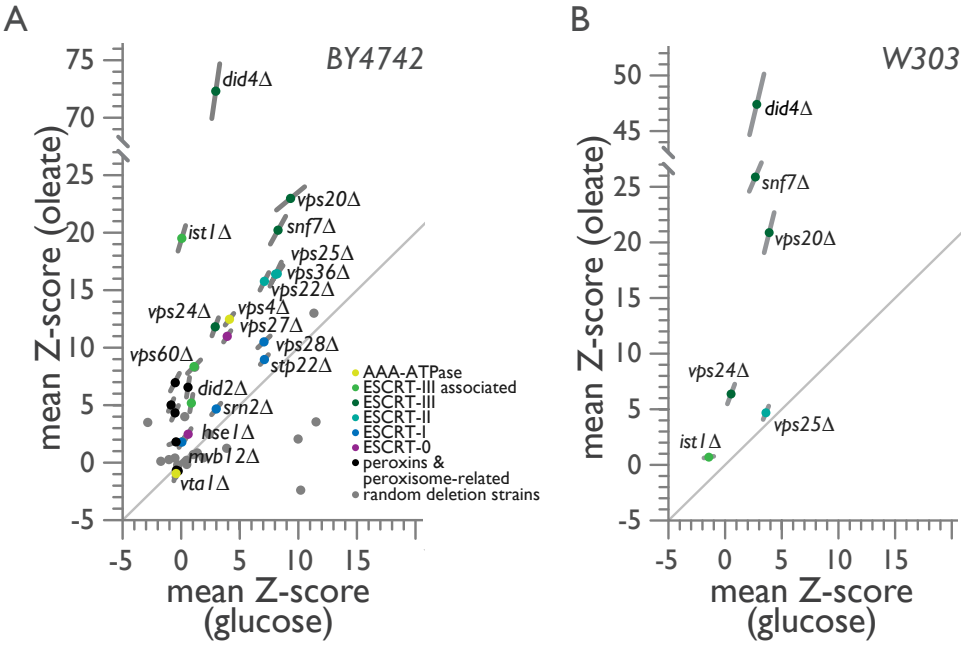

Figure 1
Mast et al., 2018

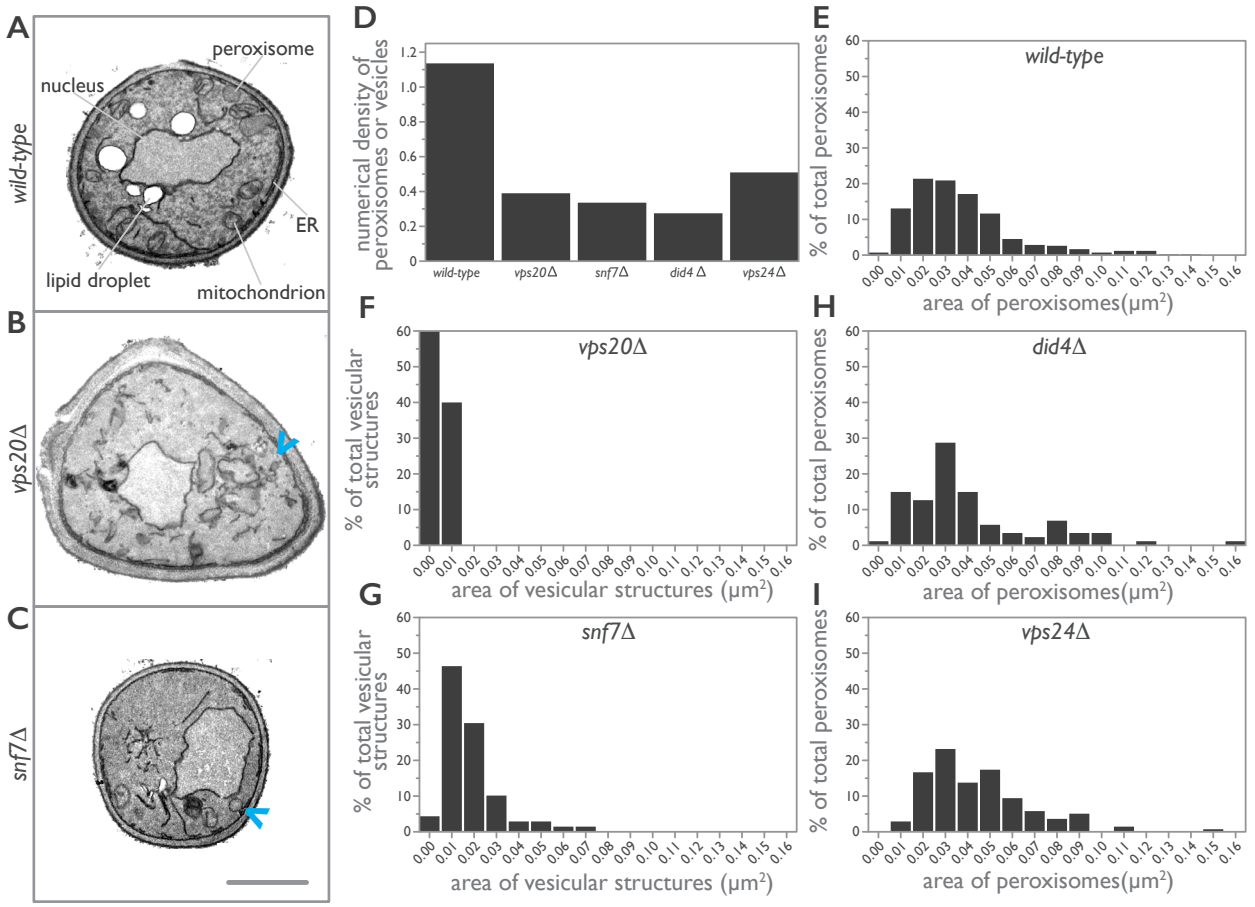

Figure 2
Mast et al., 2018

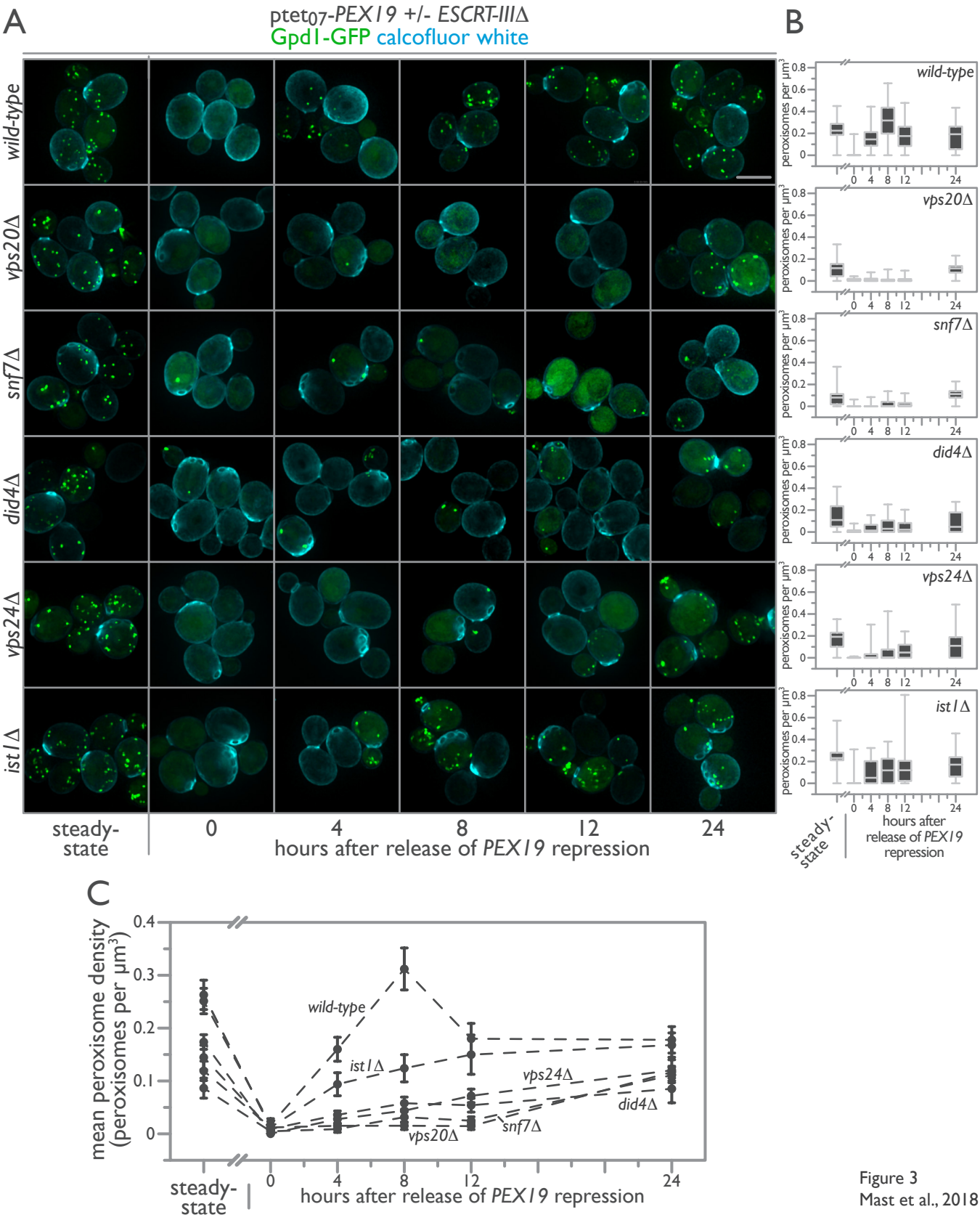

Figure 3
Mast et al., 2018

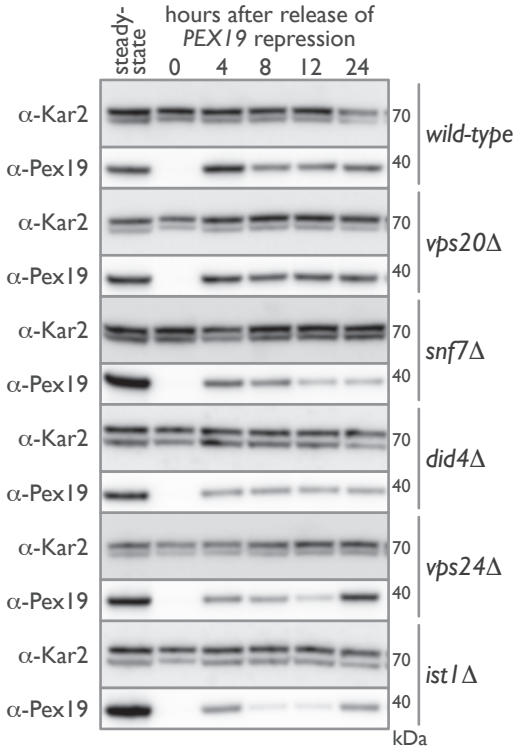

Figure 4
Mast et al., 2018

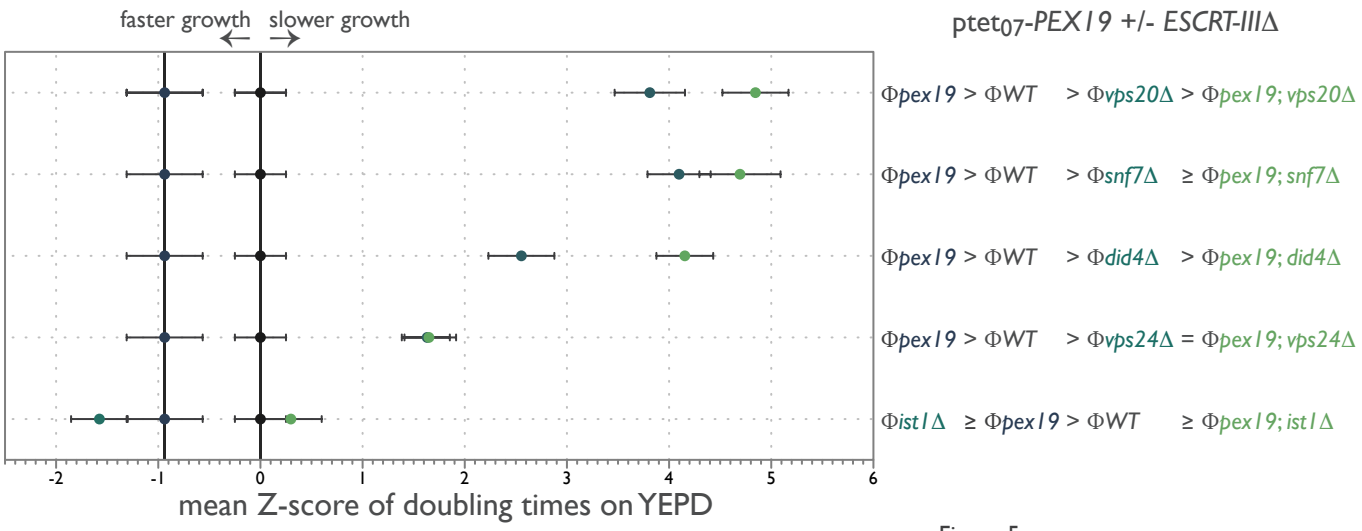

Figure 5
Mast et al., 2018

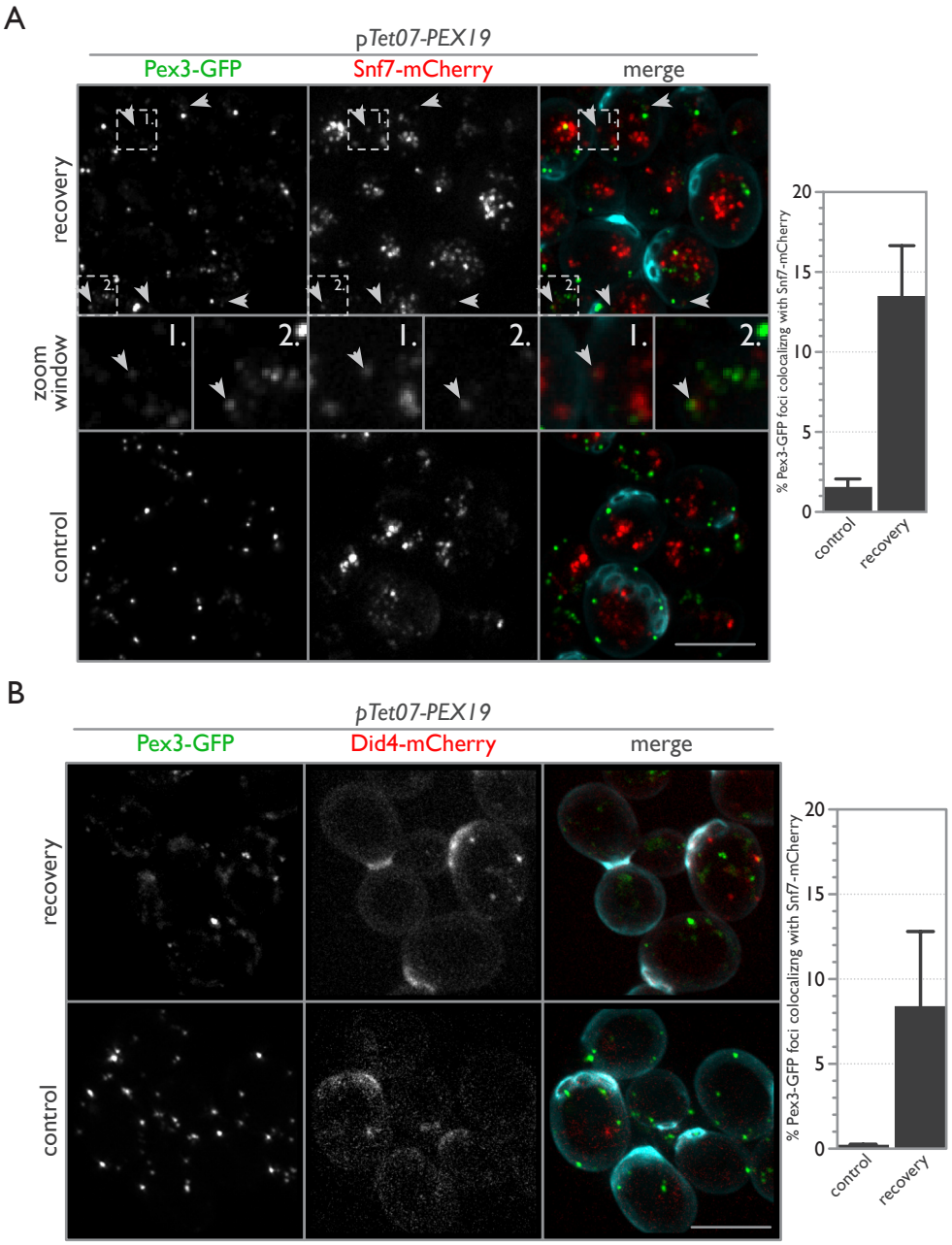

Figure 6
Mast et al., 2018

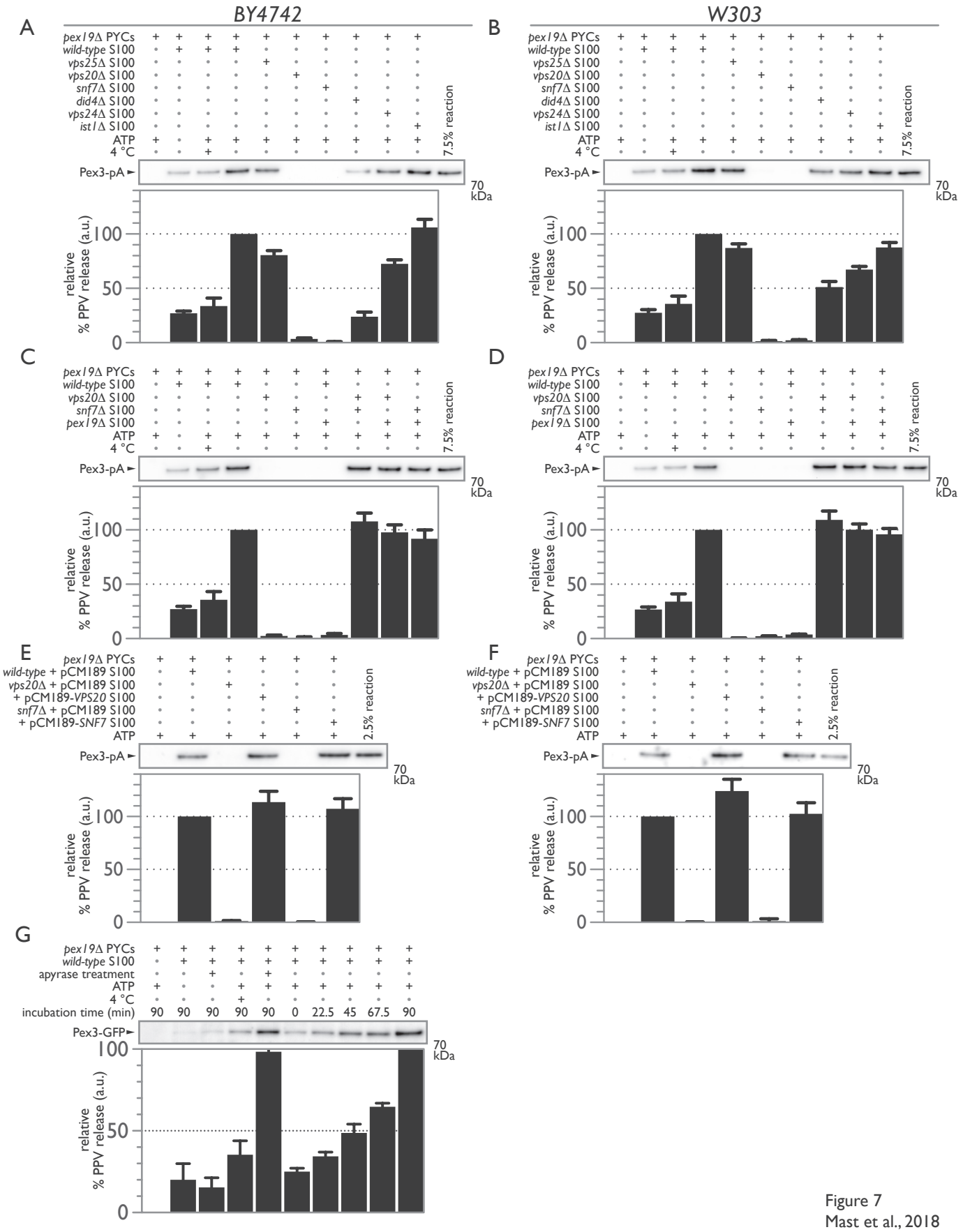

Figure 7
Mast et al., 2018